Thermalization and light cones in a model with weak integrability breaking

Bruno Bertini,[1,2] Fabian H.L. Essler,[1] Stefan Groha,[1] and Neil J. Robinson[3]

[1] *The Rudolf Peierls Centre for Theoretical Physics, University of Oxford, Oxford, OX1 3NP, United Kingdom*
[2] *SISSA and INFN, Sezione di Trieste, via Bonomea 265, I-34136, Trieste, Italy*
[3] *Condensed Matter Physics and Materials Science Division, Brookhaven National Laboratory, Upton, New York 11973, USA*

(Dated: November 10, 2016)

We employ equation of motion techniques to study the non-equilibrium dynamics in a lattice model of weakly interacting spinless fermions. Our model provides a simple setting for analyzing the effects of weak integrability breaking perturbations on the time evolution after a quantum quench. We establish the accuracy of the method by comparing results at short and intermediate times to time-dependent density matrix renormalization group computations. For sufficiently weak integrability-breaking interactions we always observe *prethermalization plateaux*, where local observables relax to non-thermal values at intermediate time scales. At later times a crossover towards thermal behaviour sets in. We determine the associated time scale, which depends on the initial state, the band structure of the non-interacting theory, and the strength of the integrability breaking perturbation. Our method allows us to analyze in some detail the spreading of correlations and in particular the structure of the associated light cones in our model. We find that the interior and exterior of the light cone are separated by an intermediate region, the temporal width of which appears to scale with a universal power-law $t^{1/3}$.

PACS numbers: 71.10.Fd, 05.70.Ln, 71.10.Pm, 03.75.Ss

I. INTRODUCTION

It is now well established that there is a significant difference between the nonequilibrium dynamics of integrable and nonintegrable quantum systems after a quantum quench.[1–13] Generic (nonintegrable) systems thermalize: local observables relax towards stationary values described by a Gibbs ensemble with an effective temperature set by the initial state.[14–22] Integrable systems, however, relax towards a generalized Gibbs ensemble (GGE),[23–60], which retains an infinite amount of information on the initial state.

This raises interesting questions: how does adding a weak perturbation to an integrable model affect its non-equilibrium dynamics? Does the proximity to an integrable theory influence the dynamics at finite times? In classical few-particle systems, this is a long-studied problem: a weak integrability breaking perturbation induces a fascinating crossover between nonergodic and chaotic motion, where the system retains aspects of the nonergodic integrable motion on intermediate time scales.[61] It has recently been understood that something analogous occurs in quantum many-body systems. Models with weak integrability breaking perturbations have been found to exhibit transient behaviour, in which observables relax to non-thermal values at intermediate times. This phenomenon was termed *prethermalization* (PT)[62] and has been observed in a number of models[62–79] as well as in experiments on ultra-cold bosonic gases.[11,80–83]

The general expectation is that PT is a transient phenomenon, and that at late times thermalization sets in. This is a natural assumption, but the evidence in its favor is rather scant; most of the available numerical[84] and analytical[62,67] techniques are not able to reach sufficiently late times. Recently, progress has been achieved by means of equations of motion (EOM) techniques. These methods were used to study a weakly nonintegrable model in infinitely many dimension, which was observed to thermalize.[85] Reference [75] considered a one dimensional weakly non-integrable model and showed that the single-particle Green's function exhibits PT at intermediate time scales, while at long times it eventually evolves towards a thermal stationary state. In Ref. [75] the EOM were benchmarked against time-dependent density renormalization group (t-DMRG) computations and found to be in excellent agreement for all times accessible with t-DMRG. In both of these works, at long times expectation values approach their thermal values with corrections which are exponentially small in time.

In this work, we expand on the results of Ref. [75] and study the PT–thermalization crossover in detail using EOM. In particular, we focus on studying how the time scale for thermalization depends on initial state properties, the band structure and interaction strength of the post quench Hamiltonian that governs the time-evolution. Using EOM, and their long-time simplification to a quantum Boltzmann-like equation, we can study the time-evolution from short times to the PT plateau and beyond.

This paper is organized as follows. In Sec. II we introduce the class of interacting lattice fermion models considered in the following, discuss the limits in which it describes integrable models, and review some important symmetries of the Hamiltonian. In Sec. III we discuss our protocol for inducing the non-equilibrium dynamics and the "initial conditions" this induces, and intro-

duce the central object of our study, the single-particle Green's function. Following this, we derive the equations of motion for the momentum-space two point functions in Sec. IV. In Sec. V we present results for the time evolution of the Green's function, compare the EOM results to t-DMRG computations and discuss the roles played by the next-nearest neighbour hopping and the initial state in the PT-thermalization crossover. In Sec. VI we investigate light cone effects in the time-evolving Green's function. In Sec. VII we consider the long-time limit of the EOM and show that under certain assumptions they can be reduced to a set of quantum Boltzmann-like equations. We then use these to study the thermalization time scale. Section VIII reports results on the dynamics after quantum quenches in a modified Hamiltonian that breaks the global U(1) symmetry associated with particle number conservation. PT is seen to persist in this case. We conclude in Sec. IX and cover a number of technical points in the appendices.

II. THE MODEL

We consider a three-parameter family of interacting spinless fermion models with Hamiltonian

$$H(J_2,\delta,U) = -J_1\sum_{l=1}^{L}\Big[1+(-1)^l\delta\Big]\Big(c_l^\dagger c_{l+1}+\text{H.c.}\Big) - J_2\sum_{l=1}^{L}\Big[c_l^\dagger c_{l+2}+\text{H.c.}\Big] + U\sum_{l=1}^{L} n_l n_{l+1}\ , \tag{1}$$

where we impose periodic boundary conditions $c_{L+1}\equiv c_1$. Here c_i and $c_i^\dagger$ are spinless fermion operators on site i, obeying the canonical anticommutation relations

$$\{c_i^\dagger, c_j\} = \delta_{ij}\ , \qquad \{c_i, c_j\} = 0\ . \tag{2}$$

The amplitudes J_1 and J_2 describe tunneling between nearest-neighbour and next-nearest-neighbour sites respectively, and we include a nearest-neighbour dimerization of strength $0 \le \delta < 1$. Finally there is a nearest-neighbour density-density interaction of strength U. From here on we set $J_1 = 1$ and measure energies in units of J_1.

There are several limits in which the Hamiltonian (1) becomes integrable:

1. For $U = 0$ we are dealing with a non-interacting theory, which is a particularly simple example of an integrable model.
2. If we set $\delta = J_2 = 0$, the model (1) becomes equivalent to the anisotropic spin-1/2 Heisenberg model in an external magnetic field.[86]
3. The low-energy description for $J_2 = 0$ and $\delta, U \ll 1$ is given by the quantum sine-Gordon model.[87]

We have checked by computing the level spacing statistics that the model is non-integrable away from these limits. The Hamiltonian $H(J_2,\delta,U)$ is invariant under the following transformations of the fermion operators

1. Global U(1) transformations: $\mathcal{U}(\phi)$

$$c_i \to \mathcal{U}(\phi) c_i \mathcal{U}^\dagger(\phi) = e^{\mathrm{i}\phi} c_i\ , \qquad \phi\in[0,2\pi]\ , \tag{3}$$

2. Translation by two sites: $\mathcal{T}_2$

$$c_i \to \mathcal{T}_2 c_i \mathcal{T}_2^\dagger = c_{i+2}\ , \tag{4}$$

3. Inversion with respect to any bond j: $\mathcal{B}_j$

$$c_i \to \mathcal{B}_j c_i \mathcal{B}_j^\dagger = c_{2j-i+1}\ . \tag{5}$$

In the absence of next nearest neighbour tunneling $J_2 = 0$, the model exhibits an additional *particle-hole* symmetry at half filling (one fermion per two sites)

$$c_i \to \mathcal{J} c_i \mathcal{J}^\dagger = (-1)^i c_i^\dagger\ . \tag{6}$$

We are interested in the regime of weak interactions, $U \lesssim 1$. In this case, a convenient basis for analyzing the quench dynamics is provided by diagonalizing the quadratic (non-interacting) part of the Hamiltonian. This is done by going to Fourier space (using an elementary cell with two sites) and then carrying out a Bogoliubov transformation to momentum space fermion creation and annihilation operators with anticommutation relations $\{\alpha_\mu(k), \alpha_\nu^\dagger(q)\} = \delta_{\mu\nu}\delta_{k,q}$

$$c_l = \frac{1}{\sqrt{L}}\sum_{k>0}\sum_{\eta=\pm}\gamma_\eta(l,k|\delta)\alpha_\eta(k)\ . \tag{7}$$

Here the coefficients are given by

$$\begin{aligned}\gamma_\pm(2j-1,k|\delta) &= e^{-ik(2j-1)}\ ,\\ \gamma_\pm(2j,k|\delta) &= \pm e^{-ik2j}e^{-i\varphi_k(\delta)}\ ,\end{aligned} \tag{8}$$

where $\varphi_k(\delta)$ is the Bogoliubov angle

$$e^{-i\varphi_k(\delta)} = \frac{-\cos k + i\delta\sin k}{\sqrt{\cos^2 k + \delta^2\sin^2 k}}\ . \tag{9}$$

In terms of the two species of Bogoliubov fermions the Hamiltonian reads

$$H(J_2,\delta,U)=\sum_{\eta=\pm}\sum_{k>0}\epsilon_\eta(k)\alpha^\dagger_\eta(k)\alpha_\eta(k)+U\sum_{\boldsymbol{\eta}}\sum_{\boldsymbol{k}>0}V_{\boldsymbol{\eta}}(\boldsymbol{k})\alpha^\dagger_{\eta_1}(k_1)\alpha^\dagger_{\eta_2}(k_2)\alpha_{\eta_3}(k_3)\alpha_{\eta_4}(k_4)\ , \tag{10}$$

where we introduced notations $\boldsymbol{\eta}=(\eta_1,\eta_2,\eta_3,\eta_4)$, $\boldsymbol{k}=(k_1,k_2,k_3,k_4)$ and $\boldsymbol{k}>0$ is shorthand for $k_i>0$ for all $i=1,\ldots,4$. The single particle dispersion relation is

$$\epsilon_\eta(k)=-2J_2\cos(2k)+2\eta\sqrt{\delta^2+(1-\delta^2)\cos^2(k)}\ , \tag{11}$$

while the interaction $V_{\boldsymbol{\eta}}(\boldsymbol{k})$ can be written in a convenient antisymmetrized form

$$V_{\boldsymbol{\eta}}(\boldsymbol{k})=-\frac{1}{4}\sum_{P,Q\in S_2}\mathrm{sgn}(P)\mathrm{sgn}(Q)V'_{\eta_{p_1}\eta_{q_1}\eta_{p_2}\eta_{q_2}}(k_{p_1},k_{q_1},k_{p_2},k_{q_2})\ . \tag{12}$$

Here $P=(p_1,p_2)$ and $Q=(q_1,q_2)$ are permutations of $(1,2)$ and $(3,4)$ respectively and

$$\begin{aligned}V'_{\boldsymbol{\eta}}(\boldsymbol{k})=\frac{e^{i(k_3-k_4)}}{2L}\ \Big[\ &\left(\eta_1\eta_2e^{i\varphi_{k_1}(\delta)-i\varphi_{k_2}(\delta)}+\eta_3\eta_4e^{i\varphi_{k_3}(\delta)-i\varphi_{k_4}(\delta)}\right)\delta_{k_1-k_2+k_3-k_4,0}\\&+\left(\eta_1\eta_2e^{i\varphi_{k_1}(\delta)-i\varphi_{k_2}(\delta)}-\eta_3\eta_4e^{i\varphi_{k_3}(\delta)-i\varphi_{k_4}(\delta)}\right)\delta_{k_1-k_2+k_3-k_4\pm\pi,0}\Big]\ .\end{aligned} \tag{13}$$

III. QUANTUM QUENCH

A. Quench Protocol

Our protocol for inducing and analyzing nonequilibrium dynamics is as follows. We always prepare the system in an initial density matrix ρ_0 that is "not an eigenstate of $H(J_2,\delta_f,U)$" for any value of U [*i.e.*, it does not commute with $H(J_2,\delta_f,U)$]. An important condition we impose is that Wick's theorem holds in the initial density matrix. A convenient choice we use in the following is provided by the equilibrium states

$$\rho_0(\beta_i,\delta_i)=\frac{e^{-\beta_iH(0,\delta_i,0)}}{\mathrm{Tr}[e^{-\beta_iH(0,\delta_i,0)}]}\ , \tag{14}$$

These states include, as a particular case, the ground state of the Hamiltonian $H(0,\delta_i,0)$. The rationale for considering finite temperatures $\beta_i<\infty$ is that this provides us with a simple way of changing the energy density in the initial state.

1. *Integrable quench*

One class of quenches we consider is to the noninteracting theory with Hamiltonian $H(J_2,\delta_f,0)$. The time evolved density matrix in this case is

$$\rho(t)=e^{-itH(J_2,\delta_f,0)}\rho_0e^{itH(J_2,\delta_f,0)}\ . \tag{15}$$

2. *Integrability breaking quench*

The second class of quenches we consider is to the nonintegrable theory with Hamiltonian $H(J_2,\delta_f,U)$. The time evolved density matrix in this case is

$$\rho(t)=e^{-itH(J_2,\delta_f,U)}\rho_0e^{itH(J_2,\delta_f,U)}\ . \tag{16}$$

Here the interaction with strength U plays the role of a weak integrability-breaking perturbation, and our aim is to quantify how this perturbation changes the dynamics compared to the integrable quench.

We stress that our protocol differs in a very important way from weak interaction quenches which have been analyzed previously with equations of motion techniques.[85,88] In these cases, no dynamics are present for $U=0$; hence quenching the interaction from zero to a finite value simultaneously induces a time dependence in the problem *and* breaks the integrability. Accordingly, the effect of the integrability breaking on the nonequilibrium dynamics is masked.

B. The single-particle Green's function

The main object of interest in this work is the single-particle Green's function

$$\mathcal{G}(j,l;t)=\mathrm{Tr}\left[\rho(t)c^\dagger_jc_l\right]. \tag{17}$$

From the symmetries of the Hamiltonian (and hence those of the initial state (14)), the following properties of the Green's function can be derived

$$\mathcal{G}(j,l;t)=\mathcal{G}(j+2n,l+2n;t)\ , \tag{18}$$

$$\mathcal{G}(j,l;t)=\mathcal{G}(j,l;t)^*\ ,\qquad j-l=2n+1\ , \tag{19}$$

$$\mathcal{G}(j,l;t)=\mathcal{G}(j,2j-l;t)^*\ ,\qquad j-l=2n\ , \tag{20}$$

where n is an integer. The Green's function can be obtained from the two-point functions of the Bogoliubov fermion operators $\alpha_\pm(k)$ of the final Hamiltonian $H(J_2,\delta_f,U)$

$$\mathcal{G}(j,l;t)=\frac{1}{L}\sum_{k>0}\sum_{\mu,\nu=\pm}\gamma^*_\mu(k,j)\gamma_\nu(k,l)n_{\mu\nu}(k,t)\,, \tag{21}$$

where we have defined

$$n_{\mu\nu}(k,t) = \mathrm{Tr}\left[\rho(t)\alpha^\dagger_\mu(k)\alpha_\nu(k)\right] \ . \tag{22}$$

Since ρ_0 is noninteracting, we can easily evaluate (22) for $t=0$

$$n_{\mu\mu}(k) = \frac{1}{2} - \frac{1}{2}\cos\big(\Delta\varphi_k(\delta_f,\delta_i)\big)\tanh\left(\frac{\beta\epsilon^{(0)}_\mu(k)}{2}\right) \ , \tag{23}$$

$$n_{\mu\bar{\mu}}(k) = \frac{i}{2}\sin\big(\Delta\varphi_k(\delta_f,\delta_i)\big)\tanh\left(\frac{\beta\epsilon^{(0)}_\mu(k)}{2}\right) \ . \tag{24}$$

Here $\Delta\varphi_k(\delta_f,\delta_i) \equiv \varphi_k(\delta_f) - \varphi_k(\delta_i)$ and the dispersion relations $\epsilon^{(0)}_\alpha(k)$ are given by (11) with $J_2 = 0$ and $\delta = \delta_i$. We note that as a consequence of the inversion symmetry (5) $\mathrm{Re}[\mathcal{G}(j,j+2n;t)]$ depends only on the occupation numbers $n_{\mu\mu}(k;t)$.

IV. EQUATIONS OF MOTION

To study the time-evolution of the Green's function we use EOM techniques.[75,85,88–90,94] In this section, for the purpose of completeness, we present the derivation of the EOM. We will closely follow the derivation given in the Supplemental Material of Ref. [75] which is in turn based on the one given in Ref. [90], where the EOM are used as an intermediate step to derive a quantum Boltzmann Equation. Our starting point is the Heisenberg equations for the time-evolved bilinears $\hat{n}_{\mu\nu}(k,t) = \alpha^\dagger_\mu(k,t)\alpha_\nu(k,t)$, which read

$$\frac{\partial}{\partial t}\hat{n}_{\mu\nu}(k,t) = i\big[H,\hat{n}_{\mu\nu}(k,t)\big] = i\epsilon_{\mu\nu}(k)\hat{n}_{\mu\nu}(k,t) + iU\sum_{\boldsymbol{\eta}}\sum_{\boldsymbol{q}>0} Y^{\boldsymbol{\eta}}_{\mu\nu}(k,\boldsymbol{q})\hat{A}_{\boldsymbol{\eta}}(\boldsymbol{q},t) \ , \tag{25}$$

Here we have defined the functions $\epsilon_{\mu\nu}(k) \equiv \epsilon_\mu(k) - \epsilon_\nu(k)$,

$$Y^{\boldsymbol{\eta}}_{\mu\nu}(k,\boldsymbol{q}) \equiv \delta_{\nu,\eta_4}\delta_{k,q_4}V_{\eta_1\eta_2\eta_3\mu}(\boldsymbol{q}) + \delta_{\nu,\eta_3}\delta_{k,q_3}V_{\eta_1\eta_2\mu\eta_4}(\boldsymbol{q}) - \delta_{\mu,\eta_2}\delta_{k,q_2}V_{\eta_1\nu\eta_3\eta_4}(\boldsymbol{q}) - \delta_{\mu,\eta_1}\delta_{k,q_1}V_{\nu\eta_2\eta_3\eta_4}(\boldsymbol{q}) \ , \tag{26}$$

and the operators

$$\hat{A}_{\boldsymbol{\eta}}(\boldsymbol{q},t) \equiv \alpha^\dagger_{\eta_1}(q_1,t)\alpha^\dagger_{\eta_2}(q_2,t)\alpha_{\eta_3}(q_3,t)\alpha_{\eta_4}(q_4,t) \ . \tag{27}$$

The quartic operators in (25) evolve according to the following Heisenberg equations of motion

$$\frac{\partial}{\partial t}\hat{A}_{\boldsymbol{\eta}}(\boldsymbol{q},t) = iE_{\boldsymbol{\eta}}(\boldsymbol{q})\hat{A}_{\boldsymbol{\eta}}(\boldsymbol{q},t) + iU\sum_{\boldsymbol{\gamma}}\sum_{\boldsymbol{p}>0} V_{\boldsymbol{\gamma}}(\boldsymbol{p})\left[\hat{A}_{\boldsymbol{\gamma}}(\boldsymbol{p},t),\hat{A}_{\boldsymbol{\eta}}(\boldsymbol{q},t)\right] \ , \tag{28}$$

where $E_{\boldsymbol{\eta}}(\boldsymbol{q}) \equiv \epsilon_{\eta_1}(q_1) + \epsilon_{\eta_2}(q_2) - \epsilon_{\eta_3}(q_3) - \epsilon_{\eta_4}(q_4)$. The commutator on the right-hand side produces operators involving six fermion creation and annihilation operators. Continuing this procedure leads to an infinite hierarchy of coupled equations. This hierarchy is closely related to the equations of motion for the reduced density operator obtained in the BBGKY approach, see e.g. Ref. [91]. The relation between the two follows directly from the Fock space representation for the reduced density operators

$$\langle k'_n\eta'_n,\ldots,k'_1\eta'_1|F_n|k_1\eta_1,\ldots,k_n\eta_n\rangle = \frac{\mathrm{Tr}\left[\rho(t)\alpha^\dagger_{\eta_1}(k_1)\ldots\alpha^\dagger_{\eta_n}(k_n)\alpha_{\eta'_n}(k'_n)\ldots\alpha_{\eta'_1}(k'_1)\right]}{n!L^n\langle N\rangle(\langle N\rangle-1)\cdots(\langle N\rangle-n)} \ . \tag{29}$$

Here F_n is the n-particle reduced density operators, obtained by tracing out the degrees of freedom associated with all but n particles from the density matrix $\rho(t)$, and $\langle N\rangle \equiv \mathrm{Tr}[\rho(t)N] = \mathrm{Tr}[\rho(0)N]$ where N is the particle-number operator. We also defined

$$|k_1\eta_1,\ldots,k_n\eta_n\rangle = \alpha^\dagger_{\eta_1}(k_1)\ldots\alpha^\dagger_{\eta_n}(k_n)\,|0\rangle \ , \tag{30}$$

where $|0\rangle$ the vacuum state, satisfying $\alpha_\eta(k)\,|0\rangle = 0$ for all k and η. From Eq. (29) we see that the expectation values of strings of fermionic operators that appear in our hierarchy are essentially the matrix elements of the reduced density operators. In particular, by taking the expectation value of (25) and (28) we recover the first two equations of the BBGKY hierarchy.

In order to proceed we integrate (28) in time and then take the expectation value in our initial state ρ_0. This gives

$$\langle\hat{A}_{\boldsymbol{\eta}}(\boldsymbol{q},t)\rangle = \langle\hat{A}_{\boldsymbol{\eta}}(\boldsymbol{q},0)\rangle\, e^{itE_{\boldsymbol{\eta}}(\boldsymbol{q})} + iU\sum_{\boldsymbol{\gamma}}\sum_{\boldsymbol{p}>0}\int_0^t \mathrm{d}s\ e^{i(t-s)E_{\boldsymbol{\eta}}(\boldsymbol{q})}V_{\boldsymbol{\gamma}}(\boldsymbol{p})\left\langle\left[\hat{A}_{\boldsymbol{\gamma}}(\boldsymbol{p},s),\hat{A}_{\boldsymbol{\eta}}(\boldsymbol{q},s)\right]\right\rangle \ , \tag{31}$$

where we have defined $\langle \hat{O} \rangle \equiv \mathrm{Tr}[\rho_0 \hat{O}]$. Taking the expectation value of Eq. (25) in ρ_0 and then using (31), we obtain a set of exact integro-differential equations for the expectation values $n_{\mu\nu}(k,t) = \mathrm{Tr}[\rho_0 \hat{n}_{\mu\nu}(k,t)]$ (see Eq. (22))

$$\begin{aligned}\frac{\partial}{\partial t} n_{\mu\nu}(k,t) =& i\epsilon_{\mu\nu}(k) n_{\mu\nu}(k,t) + iU \sum_{\boldsymbol{\eta}} \sum_{\boldsymbol{q}>0} Y^{\boldsymbol{\eta}}_{\mu\nu}(k,\boldsymbol{q}) \langle \hat{A}_{\boldsymbol{\eta}}(\boldsymbol{q},0) \rangle e^{itE_{\boldsymbol{\eta}}(\boldsymbol{q})} \\ & - U^2 \sum_{\boldsymbol{\eta},\boldsymbol{\gamma}} \sum_{\boldsymbol{q},\boldsymbol{p}>0} \int_0^t \mathrm{d}s \; Y^{\boldsymbol{\eta}}_{\mu\nu}(k,\boldsymbol{q}) e^{i(t-s)E_{\boldsymbol{\eta}}(\boldsymbol{q})} V_{\boldsymbol{\gamma}}(\boldsymbol{p}) \langle \hat{A}_{\boldsymbol{\gamma}}(\boldsymbol{p},s) \hat{A}_{\boldsymbol{\eta}}(\boldsymbol{q},s) \rangle \\ & + U^2 \sum_{\boldsymbol{\eta},\boldsymbol{\gamma}} \sum_{\boldsymbol{q},\boldsymbol{p}>0} \int_0^t \mathrm{d}s \; Y^{\boldsymbol{\gamma}}_{\mu\nu}(k,\boldsymbol{p}) e^{i(t-s)E_{\boldsymbol{\gamma}}(\boldsymbol{p})} V_{\boldsymbol{\eta}}(\boldsymbol{q}) \langle \hat{A}_{\boldsymbol{\gamma}}(\boldsymbol{p},s) \hat{A}_{\boldsymbol{\eta}}(\boldsymbol{q},s) \rangle \, . \end{aligned} \tag{32}$$

Since we focus on cases where Wick's theorem holds for the initial density matrix ρ_0, see Eq. (14), the expectation value $\langle \hat{A}_{\boldsymbol{\alpha}}(\boldsymbol{q},0) \rangle$ can be written in terms of the initial values $n_{\mu\nu}(k,0)$. The time-dependent eight-point average present in Eq. (32) can be decomposed into the form

$$\langle \hat{A}_{\boldsymbol{\gamma}}(\boldsymbol{p},t) \hat{A}_{\boldsymbol{\alpha}}(\boldsymbol{q},t) \rangle = f(\{n_{\mu\nu}(k,t)\}) + \mathcal{C}[\langle \hat{A}_{\boldsymbol{\gamma}}(\boldsymbol{p},t) \hat{A}_{\boldsymbol{\alpha}}(\boldsymbol{q},t) \rangle] \, , \tag{33}$$

where f represents the fully disconnected part (which is obtained by applying Wick's theorem), and $\mathcal{C}[\cdots]$ denotes terms involving the four, six and eight-particle cumulants [the eight particle cumulant does not contribute to Eq. (32) due to the antisymmetric structure of the accompanying term]. In order for Eq. (32) to reduce to a closed set of integro-differential equations, we now assume that the four and six particle cumulants are negligible at all times. This assumption is uncontrolled – we check it by comparison of our results to those obtained using t-DMRG (it will be apparent that this assumption is valid for the model and initial conditions under consideration). This truncation leads a closed system of equations for the expectation values

$$\begin{aligned}\frac{\partial}{\partial t} n_{\mu\nu}(k,t) =& i\epsilon_{\mu\nu}(k) n_{\mu\nu}(k,t) + 4iU \sum_{\gamma_1\gamma_2\gamma_3} \sum_{q>0} V_{\gamma_1\gamma_2\gamma_3\mu}(k,q,q,k) e^{i\epsilon_{\gamma_1\nu}(k)t} e^{i\epsilon_{\gamma_2\gamma_3}(q)t} n_{\gamma_1\nu}(k,0) n_{\gamma_2\gamma_3}(q,0) \\ & - 4iU \sum_{\gamma_1\gamma_2\gamma_3} \sum_{q>0} V_{\nu\gamma_2\gamma_3\gamma_1}(k,q,q,k) e^{i\epsilon_{\mu\gamma_1}(k)t} e^{i\epsilon_{\gamma_2\gamma_3}(q)t} n_{\mu\gamma_1}(k,0) n_{\gamma_2\gamma_3}(q,0) \\ & - U^2 \int_0^t \mathrm{d}t' \sum_{\vec{\gamma}} \sum_{k_1,k_2,k_3>0} L^{\vec{\gamma}}_{\mu\nu}(k_1,k_2,k_3;k;t-t') n_{\gamma_1\gamma_2}(k_1,t') n_{\gamma_3\gamma_4}(k_2,t') n_{\gamma_5\gamma_6}(k_3,t') \\ & - U^2 \int_0^t \mathrm{d}t' \sum_{\boldsymbol{\gamma}} \sum_{k_1,k_2>0} K^{\boldsymbol{\gamma}}_{\mu\nu}(k_1,k_2;k;t-t') n_{\gamma_1\gamma_2}(k_1,t') n_{\gamma_3\gamma_4}(k_2,t') \, . \end{aligned} \tag{34}$$

Here we have introduced notations such that $\vec{\gamma} = (\gamma_1 \ldots \gamma_6)$ and the kernels are given by

$$\begin{aligned} K^{\boldsymbol{\gamma}}_{\mu\nu}(k_1,k_2;k;t) &= 4 \sum_{k_3,k_4>0} \sum_{\eta,\eta'} X^{\gamma_1\gamma_3\eta\eta';\eta\eta'\gamma_4\gamma_2}_{\boldsymbol{k};\boldsymbol{k}'}(\mu,\nu;k;t), \\ L^{\vec{\gamma}}_{\mu\nu}(k_1,k_2,k_3;k;t) &= 8 \sum_{\eta} \sum_{k_4>0} X^{\gamma_1\gamma_3\gamma_6\eta;\eta\gamma_5\gamma_4\gamma_2}_{\boldsymbol{k};\boldsymbol{k}'}(\mu,\nu;k;t) - 16 \sum_{\eta} X^{\gamma_1\gamma_3\eta\gamma_4;\gamma_5\eta\gamma_6\gamma_2}_{k_1k_2k_1k_2;k_3k_1k_3k_1}(\mu,\nu;k;t) \, , \\ X^{\boldsymbol{\gamma};\boldsymbol{\eta}}_{\boldsymbol{k};\boldsymbol{q}}(\mu,\nu;q;t) &= Y^{\boldsymbol{\gamma}}_{\mu\nu}(\boldsymbol{k},q) V_{\boldsymbol{\eta}}(\boldsymbol{q}) e^{iE_{\boldsymbol{\gamma}}(\boldsymbol{k})t} - (\boldsymbol{\gamma},\boldsymbol{k}) \leftrightarrow (\boldsymbol{\eta},\boldsymbol{q}). \end{aligned} \tag{35}$$

In the framework of the BBGKY approach, our truncation scheme is sometimes referred to as the *second Born approximation*.[91] We note that the same result can be obtained in the non-equilibrium Green's function approach,[92] as discussed in Ref. [93].

It is useful to note that our truncation scheme and Eqs. (34) conserve the total energy

$$\begin{aligned} E =& \sum_{\eta=\pm} \sum_{k>0} \epsilon_{\eta}(k) n_{\eta\eta}(k,t) + U \sum_{\boldsymbol{\eta}} \sum_{\boldsymbol{k}>0} V_{\boldsymbol{\eta}}(\boldsymbol{k}) \langle \hat{A}_{\boldsymbol{\eta}}(\boldsymbol{k},0) \rangle e^{itE_{\boldsymbol{\eta}}(\boldsymbol{k})} \\ & + iU \sum_{\boldsymbol{\gamma},\boldsymbol{\eta}} \sum_{\boldsymbol{k},\boldsymbol{p}>0} \int_0^t \mathrm{d}s \; e^{i(t-s)E_{\boldsymbol{\eta}}(\boldsymbol{q})} V_{\boldsymbol{\eta}}(\boldsymbol{k}) V_{\boldsymbol{\gamma}}(\boldsymbol{p}) f(\{n_{\mu\nu}(k,t)\}) \, , \end{aligned} \tag{36}$$

where $f(\{n_{\mu\nu}(k,t)\})$ is the Wick's theorem part of $\langle \hat{A}_{\boldsymbol{\gamma}}(\boldsymbol{p},t) \hat{A}_{\boldsymbol{\alpha}}(\boldsymbol{q},t) \rangle$ appearing in (33).

Solving the system of integro-differential equations (34) is computationally demanding; we designed an algorithm which scales as $L^3 \times T$, where T is the number

of time steps and L the number of lattice sites. Our algorithm is based on the following idea: we store the values of the integrals in variables of the form

$$I_{\alpha_1\ldots\alpha_j}(k_1,k_2,k_3;t) = \int_0^t \mathrm{d}s\; F_{\alpha_1\ldots\alpha_j}(k_1,k_2,k_3;s), \quad (37)$$

where $F(k_1,k_2,k_3;s)$ contains products of $n_{\mu\nu}(k_j,t)$, vertex functions and oscillating phases $e^{i\epsilon_{\mu\nu}(k)t}$; then we solve the extended system of equations for $\{n_{\mu\nu}(k,t)\}$ and $\{I(k_1,k_2,k_3;t)\}$ by means of a fourth-order Runge-Kutta method.[95] Using this procedure we can reach long times $J_1 t \sim 100$ on large systems $L \sim 400$ (an algorithm with similar scaling was proposed in Ref. [88]). The maximum times that we consider are controlled by the appearance of finite-size related traversals.[7]

A. Window of applicability

Truncating the Green's function hierarchy is an uncontrolled approximation and an important question is: in what parameter regime we may expect it to be accurate? A crucial aspect of our work is that we always initialize the system in states where the neglected cumulants vanish. This means that for small U and short times the EOMs will provide a good approximation. We have verified this by independent checks, *cf.* Sec. V. Over time the higher cumulants may grow and eventually become important. If this happens, our approach will cease to be quantitatively accurate. The basic premise of our work is to apply the EOM approach to some intermediate time window. The behaviour at asymptotically late times may well show features not captured by our method.[96,97]

B. Leading order approximation

The EOM (34) that we have derived are the result of a second order expansion in the interaction parameter U: we approximately take into account the effect of the four-particle connected cumulants in the expectation value of Eq. (25) with respect to the initial density matrix ρ_0 by means of Eqs. (31). A less accurate 'leading order' approximation would be to neglect all four-particle cumulants from the expectation value of (25): this gives rise to a simpler system of equations, which read

$$\begin{aligned}\frac{\partial}{\partial t} n_{\mu\nu}(k,t) =& i\epsilon_{\mu\nu}(k) n_{\mu\nu}(k,t) \\ &+ 4iU \sum_{\gamma_1\gamma_2\gamma_3} \sum_{q>0} \Big[V_{\gamma_1\gamma_2\gamma_3\mu}(k,q,q,k) n_{\gamma_1\nu}(k,t) n_{\gamma_2\gamma_3}(q,t) - V_{\nu\gamma_2\gamma_3\gamma_1}(k,q,q,k) n_{\mu\gamma_1}(k,t) n_{\gamma_2\gamma_3}(q,t) \Big] . \quad (38)\end{aligned}$$

For short times, the right hand sides of Eqs. (38) and Eqs. (34) coincide with the perturbative expansion of $i\mathrm{Tr}\big[\rho_0\big[H,\hat{n}_{\mu\nu}(k,t)\big]\big]$ to first and second order in U, respectively.

Equations (38) give results which are equivalent to those found by means of the first-order continuous unitary transformation (CUT)[62,98–100] approach used in Ref. [67]. Solving the equations up to $O(U^2)$ corrections, it is easy to extract the expectation values of $\hat{n}_{\mu\nu}(k)$ in the "deformed GGE" of Ref. [67].

The EOM (34) at short times refine the leading order description (obtained by either the leading order EOM or CUT approach) by going to next order in perturbation theory. However, at later times we will see that non-perturbative feedback mechanisms present in the second order EOM cause a drifting away from the PT plateau observed in the leading order approximations.

V. THE GREEN'S FUNCTION FROM THE EQUATIONS OF MOTION

We now turn our attention to computation of the time-evolution of the Green's function (21) by means of the EOM. We first begin by providing a crucial check of the validity of the approximations underlying the EOM by direct comparison to t-DMRG computations. In Fig. 1 we report the time-evolution of $\mathcal{G}(L/2, L/2{+}1)$ computed by means of the EOM and t-DMRG for a quench in which the system is prepared in the ground state of $H(0, 0.8, 0)$ and time-evolved with $H(0, 0.4, 0.4)$. We see that, despite $U = 0.4$ being relatively large, there is remarkably good agreement between the two methods for all times accessible to the t-DMRG computations. Importantly, t-DMRG results[67] for the Green's functions at larger distances are similarly well reproduced. This agreement confirms that the EOM method is accurate for small values of U on short and intermediate time scales. The main advantage of the EOM method compared to t-DMRG is that it allows us to access larger systems and longer times than those previously reported.[67]

We observe very long-lived PT plateaux, as is exempli-

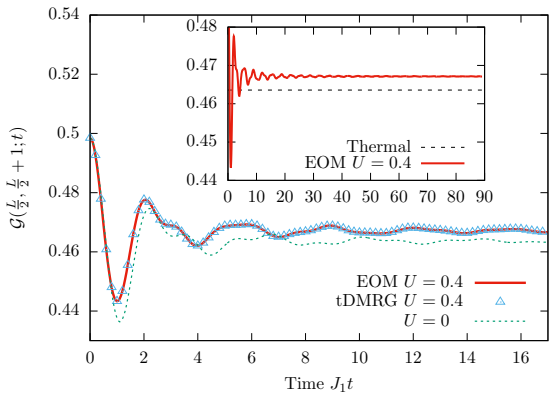

FIG. 1. Green's function $\mathcal{G}(L/2, L/2+1; t)$ on a $L = 256$ site system for a quench where the system is prepared in the ground state of $H(0, 0.8, 0)$ and time evolved with $H(0, 0.4, 0.4)$. EOM results (red line) are in excellent agreement with t-DMRG computations[67] (triangles); the green dotted line shows the result of the "integrable quench" (*i.e.* time evolution generated by $H(0, 0.4, 0)$, *cf.* Sec. III A 1). Inset: behaviour on a larger time interval.

fied in the inset of Fig. 1. There is an intermediate time window during which the Green's functions appear to settle to quasi-stationary values. These are well-separated from the thermal values, computed via exact diagonalization (ED) on a system of $L = 16$ sites. In computing the thermal values, we adopt the following procedure: we first compute the energy density in our system, given by

$$e = \frac{1}{L}\mathrm{Tr}\left[\rho_0 H(J_2, \delta_f, U)\right] \ . \tag{39}$$

We then determine the effective temperature $1/\beta_{\rm eff}$ of the thermal ensemble for the post-quench Hamiltonian $H(J_2, \delta, U)$ through

$$e \stackrel{!}{=} \frac{1}{L}\mathrm{Tr}\left[\frac{1}{Z}e^{-\beta_{\rm eff}H(J_2,\delta_f,U)}H(J_2,\delta_f,U)\right]\Big|_{\text{fixed } n} \ . \tag{40}$$

In practice we compute (40) by ED, where the trace is performed over states with a fixed particle number density $n = \mathrm{Tr}\left[\rho_0 N\right]/L$. We then compute the single-particle Green's function in thermal equilibrium at temperature $1/\beta_{\rm eff}$ using the same method. Our ED results for the thermal value of $\mathcal{G}(L/2, L/2+1)$ are consistent with the quantum Monte Carlo results reported in Ref. [67].

The quasi-stationary values to which the Green's functions relax are compatible with the CUT results of Ref. [67] up to order U^2 corrections. This means that (up to the $O(U^2)$ corrections) the stationary values can be described the "deformed GGE" ensemble,[67] which corrects the stationary values of the non-interacting GGE to $O(U)$.

A. Effects of next-nearest-neighbour hopping and finite temperature initial states.

To investigate whether the prethermalized regime eventually evolves toward thermal equilibrium, it is convenient to both invoke a non-zero next-nearest-neighbour hopping amplitude J_2, and to initialize the system in a thermal density matrix rather than a ground state. Here we focus on the thermal initial state (14) with inverse temperature $\beta_i = 2$ and $\delta_i = 0$. A detailed analysis of the dependence of the time evolution on β_i and δ_i is carried out in Sec. V C. The dependence of the dynamics of $\mathcal{G}(i, j; t)$ on the final dimerization δ_f, the sign of interaction U, and the presence of particle-hole symmetry is discussed in Appendix A.

We start by investigating the effects of a finite temperature initial state on the dynamics with $J_2 = 0$. In Fig. 2 we show results for the Green's functions $\mathcal{G}(L/2, L/2 \pm 1; t)$ for a $L = 320$ site system time-evolved with the Hamiltonian $H(0, 0.1, 0.4)$ and initially prepared in a thermal state (14) with density matrix $\rho_0(2, 0)$. We observe a very slow drift towards the thermal value (note the scale on the y-axis). This should be contrasted to starting from the ground state and $J_2 = 0$, *cf.* Fig. 1 and Ref. [67], where no drift is observed on the time scales accessible to us.

We now turn our attention to the effects of including a next-nearest-neighbour tunneling J_2 at fixed U. In Fig. 3 we report the time-evolution of the Green's function $\mathcal{G}(L/2, L/2-1)$ for the system prepared in the thermal density matrix $\rho_0(2, 0)$ defined in Eq. (14) and subsequently time-evolved with the Hamiltonian $H(J_2, 0.1, 0.4)$ for $J_2 = 0,\ 0.25,\ 0.375,\ 0.425,\ 0.5,\ 0.55,\ 0.6$. We see that the main effect of increasing J_2 at fixed U is to induce a drift off the PT plateau towards the thermal values.

For weak next-nearest-neighbour hopping the system is close to the prethermalized quasi-stationary state over

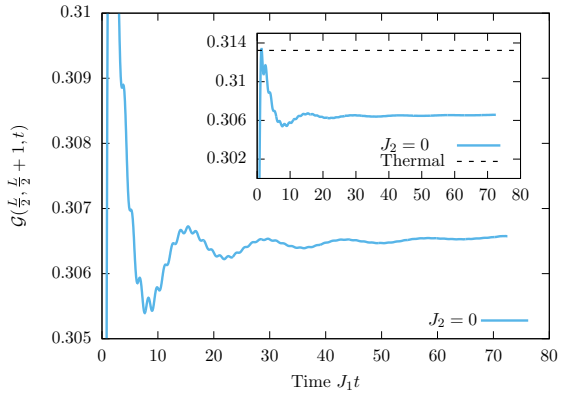

FIG. 2. Green's function $\mathcal{G}(L/2, L/2+1; t)$ for a system of size $L = 320$ prepared in state with density matrix $\rho_0(2, 0)$(14) and time-evolved with $H(0, 0.1, 0.4)$. The insets show the position of the ED thermal values.

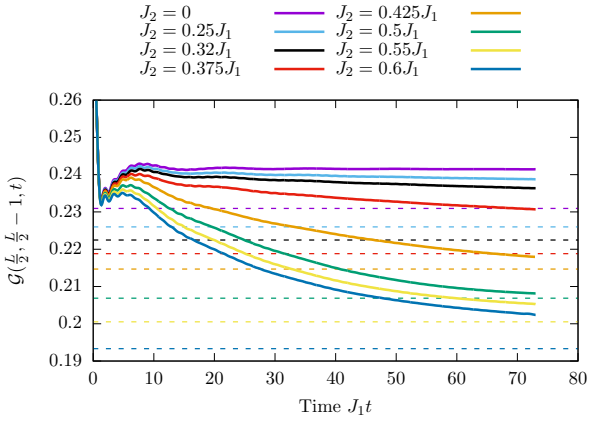

FIG. 3. Green's function $\mathcal{G}(L/2, L/2-1; t)$ for a system of size $L = 320$ prepared in state with density matrix $\rho_0(2,0)$(14) and time-evolved with $H(J_2, 0.1, 0.4)$. Dashed lines indicate the thermal values computed by ED of $L = 16$ sites. Different colours correspond to different values of $J_2 = 0, 0.25, 0.32, 0.375, 0.425, 0.5, 0.55, 0.6$ (top to bottom).

a large time interval as is illustrated in Fig. 3. Increasing the value of the J_2 causes this time window to significantly reduce and for large values of J_2 expectation values rapidly approach their thermal values. Importantly, the first order EOM remain prethermalized *for all times* and for all strengths of J_2. We stress that this does not imply that the first order EOM "do not work" for large J_2: for any given value of J_2 *we always observe a PT plateau* as long as U is sufficiently small. In this regime the first order EOM are in good agreement with those at second order. This point is illustrated in Fig. 4.

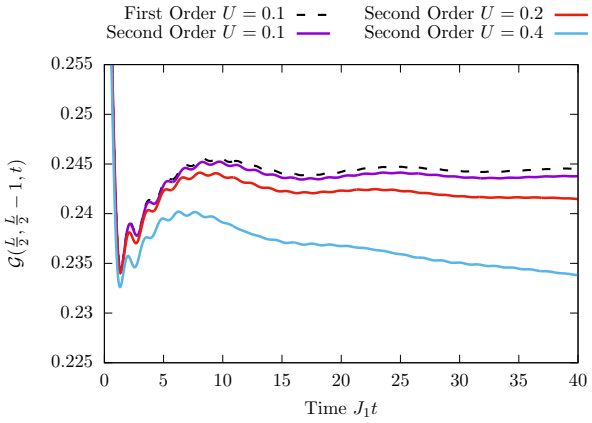

FIG. 4. Green's function $\mathcal{G}(L/2, L/2-1; t)$ for a system of size $L = 320$ prepared in the density matrix $\rho_0(2,0)$ (14) and time-evolved with $H(0.375, 0.1, U)$ for several values of U. Solid lines show results from the second order EOM (34) for $U = 0.1, 0.2, 0.4$ (top to bottom). For $U = 0.1$ we compare with the first order EOM (dashed).

In summary, *at fixed* U the addition of J_2 allows us to tune the crossover timescale between the prethermalized and thermalized regimes. Some understanding of the strong dependence on J_2 can be gained by considering $J_2 > 0.25$, where additional scattering channels open due to crossings at a fixed energy (see Fig. 5), which promotes relaxation. Figure 5 exhibits a second important effect of J_2: it changes the bandwidths $W_{1,2}$ of both bands and leads to a reduction of $W_{\min} = \min(W_1, W_2)$. This in turn leads to a larger value $U/W_{\min}$ of the dimensionless interaction strength. However, as is shown in Appendix A 1, even in cases where $W_{\min}$ is unchanged, the opening of additional scattering channels (*i.e.* increasing the number of crossings at fixed energy) is sufficient to speed up the relaxation. These findings are in accord with recent work on the relaxational dynamics in the Hubbard model[101,102] by means of quantum Boltzmann equation methods. In these works it was observed that adding a next-nearest neighbour hopping leads to thermalization.

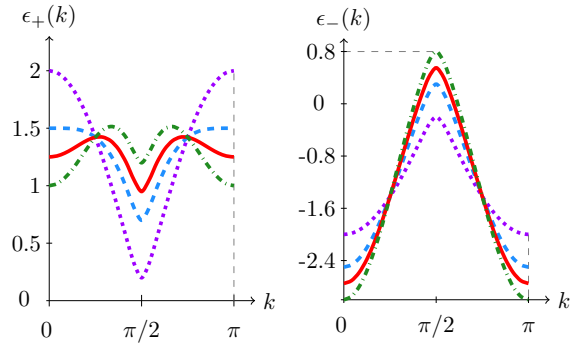

FIG. 5. Dispersion relations for the two bands of Bogoliubov fermions in the non-interacting model with $J_1 = 1$, $\delta = 0.1$ and $J_2 = 0$ (violet, dotted), $J_2 = 0.25$ (blue, dashed), $J_2 = 0.375$ (red, solid), $J_2 = 0.5$ (green, dot-dashed). Increasing J_2 leads to additional crossings at a fixed energy for $\epsilon_+(k)$. For $J_2 > 0.6$ additional crossings at fixed energy appear as the ranges of $\epsilon_+(k)$ and $\epsilon_-(k)$ overlap.

B. Beyond the prethermalization plateaux

As we have stressed before, for sufficiently small integrability breaking parameter U we always observe a PT plateau. On the other hand, by keeping U fixed and increasing J_2 we can access a regime beyond PT. Figures 6–8 show the time-evolution of the Green's function for different separations and two values of the next-nearest-neighbour hopping amplitude J_2 which generate qualitatively different evolution of the local observables. With $J_2 = 0.25$, the Green's function remains close to the value in the prethermalized state for long times, whilst for $J_2 = 0.5$ the system rapidly thermalizes. The thermal values shown in the figures are computed by ED of small systems of $L = 16$ sites. Note that the Green's function for even separations are complex and their real

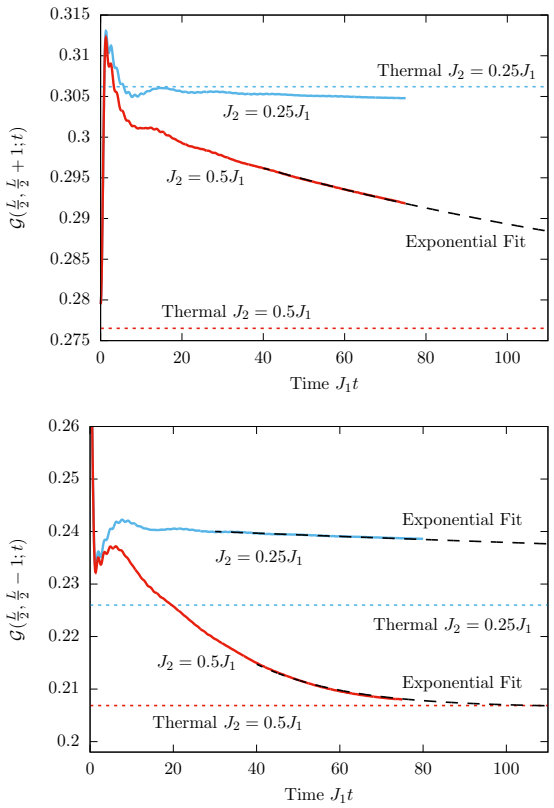

FIG. 6. Green's function $\mathcal{G}(L/2, L/2 \pm 1; t)$ for a system of size $L = 320$ prepared in state with density matrix $\rho_0(2,0)$ and time-evolved with $H(J_2, 0.1, 0.4)$. Expected steady state thermal values are shown as dotted lines, whilst the black dashed lines are exponential fits to Eq. (41). Data in the lower panel have been previously reported in Ref. [75].

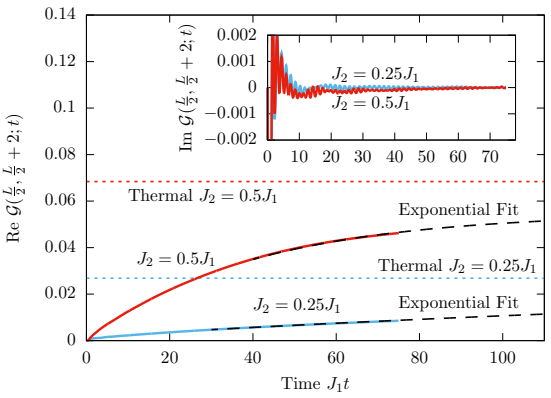

FIG. 7. Real and imaginary (inset) parts of the Green's function $\mathcal{G}(L/2, L/2+2; t)$ for a system of size $L = 320$ prepared in state with density matrix $\rho_0(2,0)$ and time-evolved with $H(J_2, 0.1, 0.4)$. Expected steady state thermal values, are shown by dotted lines while the black dashed lines are exponential fits to (41). These data have been previously reported in Ref. [75].

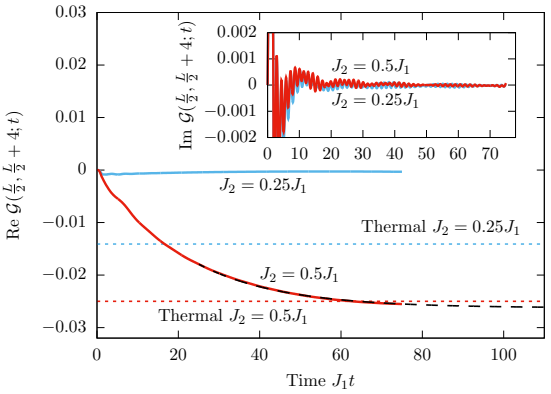

FIG. 8. Same as Fig. 7 for $\mathcal{G}(L/2, L/2+4; t)$.

parts always show a smooth behaviour in time, see for example Fig. 7. This is because they depend only on the occupation numbers $n_{\mu\mu}(k,t)$ which are slowly varying functions of time, *cf.* Section VII.

We now focus on the Green's function between sites at distances such that we observe a clear drift towards the thermal values on the time scales accessible to us, see Figs. 6, 7 and 8. The observed behaviour is compatible with an exponential decay towards the thermal value

$$\mathcal{G}(i,j;t) \sim \mathcal{G}(i,j)_{\rm th} + A_{ij}(J_2,\delta,U)e^{-t/\tau_{ij}(J_2,\delta_f,U)} \ . \quad (41)$$

Here $\mathcal{G}(i,j)_{\rm th}$ is the thermal Green's function at temperature $1/\beta_{\rm eff}$. In general the relaxation times for the real and imaginary parts of the Green's function between evenly separated sites are different, and we denote them by $\tau_{ij}(J_2,\delta_f,U)_{\rm r,i}$ in the following. In some cases, for example the $J_2 = 0.5$ case of Figs. 7 and 8, to obtain a better fit we have to allow the thermal value $\mathcal{G}(i,j)_{\rm th}$ to deviate from the ED result by a small amount. We believe that this (tiny) discrepancy can be explained by a combination of errors in the EOM and finite-size effects on the ED result.

In Fig. 9 we show the inverse relaxation times determined by fitting the decay of the Green's function to the form (41) for a system prepared in the thermal state (14) with density matrix $\rho_0(2,0)$ and time-evolved under the Hamiltonian $H(J_2, 0.1, 0.4)$ on a $L = 320$ site chain. We see that the relaxation times $\tau_{ij}(J_2,\delta_f,U)$ are quite sensitive to the value of J_2, which in turn has a large influence on whether drifting towards thermalization can be observed within the time window accessible to us. Increasing the separation between the two sites leads to an increase of the relaxation times. This takes the time window in which (41) holds beyond the regime accessible to us by a numerical solution of (34). However, we conjecture that the relation (41) describes the relaxation towards the thermal value of the Green's function for any value of the separation if one waits for long enough times. This is in some sense a "minimal" assumption: it is reasonable to think that the relaxation behaviour of the Green's function remains qualitatively the same for any separation of the two sites, providing $|i-j| \ll L$.

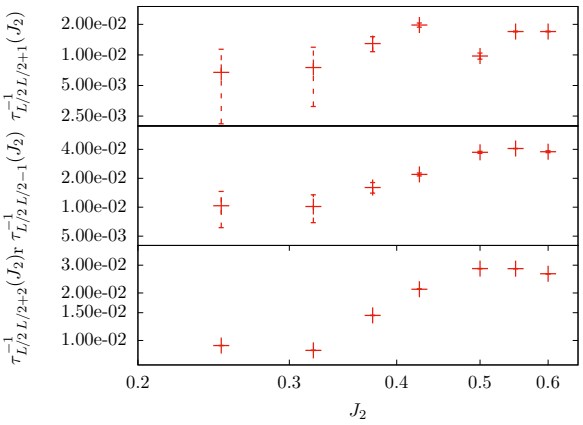

FIG. 9. Inverse relaxation times $\tau^{-1}_{L/2\,L/2+j}(J_2)$ with $j = 1, -1, 2$ (top to bottom) characterizing the late time behaviour of the Green's function (*cf.* Fig. 41). The system is prepared in the initial density matrix $\rho_0(2, 0)$ (14) and time-evolved under the Hamiltonian $H(J_2, 0.1, 0.4)$. The system size is $L = 320$ (*cf.* Fig. 3). Errors are estimated by varying the initial time at which the exponential fit is applied.

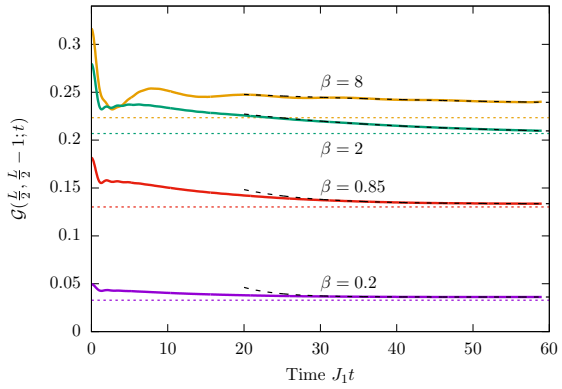

FIG. 10. $\mathcal{G}(L/2, L/2-1; t)$ for a system with Hamiltonian $H(0.5, 0.1, 0.4)$ and sizes $L = 256, 320$ initially prepared in the density matrix $\rho_0(\beta, 0)$ for four different values of β. The expected steady state thermal values are indicated by dotted lines and the exponential fit (41) by a dashed line.

In the following, we will give other arguments in favor of this conjecture by exploring the dynamics for longer times with a quantum Boltzmann equation, which can be derived as the scaling limit of the equations (34) for the occupation numbers, see Sec. VII.

C. Initial state dependence

We now turn to the dependence of the relaxation of local observables on properties of the initial state. We note that for integrable models this question has been the subject of extensive numerical studies, see for example [103–106].

1. *Dependence on the energy density*

We first consider the dependence of the relaxational behaviour on the energy density of the initial state. We note that the energy density of the various quenches we considered in Secs. V A and V B (see also Appendix A 2) was, in fact, fixed because the initial state satisfies

$$\mathrm{Tr}\,[\rho_0(\beta, 0)H(J_2, \delta, U)] = \mathrm{Tr}\,[\rho_0(\beta, 0)H(0, 0, U)]\ . \quad (42)$$

In Fig. 10 we present the time-evolution of the Green's function $\mathcal{G}(L/2, L/2-1; t)$ starting from the initial density matrices $\rho_0(\beta, 0)$ (14) with $\beta = 0.2, 0.85, 2, 8$.

Our results suggest that, fixing all other parameters, *the time window for which observables show a prethermalized behaviour increases when the temperature of the initial state is decreased* (i.e., with increasing β). In order to quantify this statement, we note that the data are well described by the "exponential relaxation" introduced in Eq. (41). We plot the inverse exponents $\tau^{-1}_{i,i-1}$ and $\tau^{-1}_{i,i+2}$ as a function of β in Fig. 11; we see that even when there is clear decrease of both exponents with β, the dependence is not of a simple power-law form. In Ref. [85], Stark and Kollar examined the limit of infinite dimensions $d \to \infty$ and found that the exponent depends on the *final* inverse temperature β_f as $\tau^{-1}_{i,j} \propto \beta_f^{-2}$. In the limit of high initial temperature $\beta_i \sim 0$, we expect the initial and final temperatures to be comparable $\beta_i \sim \beta_f$. In this limit we find a dependence $\tau^{-1}_{i\,j} \propto \beta_f^{-\alpha}$ with $\alpha \approx 0.1 - 0.2$. The different exponent compared to Ref. [85] has its origin in the distinct quench protocol as well as dimensionality.

We note that for small β the range of variation of the Green's function is very small. This is reasonable: both the initial and thermal density matrices have the form $\rho \propto \mathbb{1} + O(\beta)$, where $\mathbb{1}$ is the identity matrix. This means that to leading order in β, the expectation values do not time evolve.

2. *Different initial states at fixed energy density*

As our model is non-integrable, at late times we expect that the only relevant information contained in the initial conditions should be the energy density. Concomitantly, we expect that the Green's functions evolve towards the same limiting values when starting from macroscopically different initial states which have the same energy density. In order to investigate this point, we compare the time-evolution of the Green's function starting from the density matrix $\rho_0(\beta, \delta_i)$ for four different sets of (β, δ_i), chosen such that the energy density in each case is identical (the number density is $1/2$ in ρ_0 with $J_{2i} = 0$). By construction, these initial states are macroscopically different. As shown in Fig. 12, in each of the four cases the

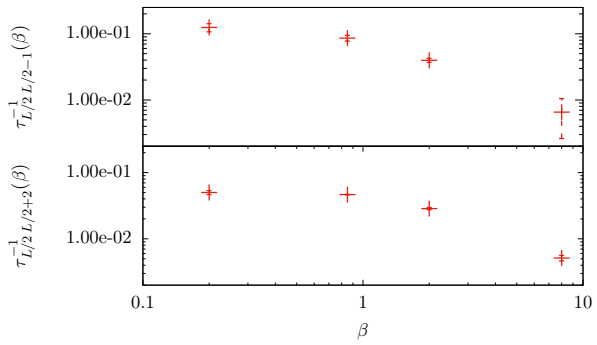

FIG. 11. Inverse Relaxation times $\tau^{-1}_{i\,i-1}(J_2,\delta,U,\beta)$ (above) and $\tau^{-1}_{i\,i+2}(J_2,\delta,U,\beta)$ (below) obtained by fitting the data in Fig. 10 with Eq. (41). Error bars are estimated by varying the initial time at which the exponential fit is applied.[107]

time evolution of Green's functions proceeds quite differently at short and intermediate times. The late time behaviour, however, appears to be compatible with the same stationary value within the errors associated with our approximations. This can be seen in the inset of Fig. 12, which shows the difference between the two most distant curves

$$d_j(i;0,0.5) = \left|\mathcal{G}(i,i+j)|_{\delta_i=0} - \mathcal{G}(i,i+j)|_{\delta_i=0.5}\right|. \quad (43)$$

We may push this analysis further by carrying out fits of

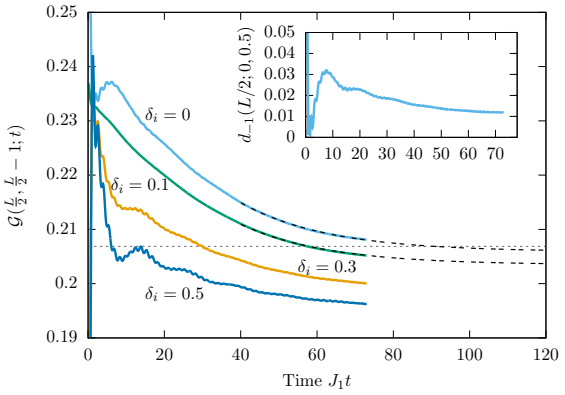

FIG. 12. $\mathcal{G}(L/2, L/2-1;t)$ for a system with Hamiltonian $H(0.5, 0.1, 0.4)$ and size $L = 320$ initially prepared in a density matrix $\rho_0(\beta,\delta_i)$, where β is chosen such that all initial states have the same energy density. Dashed lines show the exponential fit (41). Grey dotted lines indicate the thermal values computed by ED. The insets show the behaviour of $d_j(i;0,0.5)$ [*cf.* Eq. (43)].

the EOM results to the exponential form (41), and then extrapolating to late times. In cases where the relaxation is fast, e.g. $\delta_i = 0, 0.1$), we find that the extrapolated "stationary values" are in good agreement with one another and the expected thermal result computed by ED on $L = 16$ sites (the differences are $\sim 10^{-3}$). For larger values of δ_i the relaxation is slower and the extrapolated values differ significantly from the thermal result. This is perhaps not surprising, as the quality of the exponential fit is not expected to be as good in these cases. We note that the case with $\delta_i = \delta_f = 0.1$ is very similar to the one considered in Ref. [88].

VI. LIGHT CONE EFFECTS

The CUT approach[62,67] to quantum quenches provides a simple intuitive picture of PT. Switching on weak interactions does not immediately destroy the free (non-interacting) quasi-particles, but rather "dresses" them through particle-hole excitations. To leading order in U this deforms their dispersion, and higher orders will generate quasi-particle decay and render their lifetime finite. This picture propounds the idea that deviations from the PT plateau and eventual relaxation to a thermal state may be related to quasi-particle decay at finite energy densities. A very direct probe of quasi-particle propagation is provided by light cone effects.[4,7,9,10,26,31,108–120] We expect the Green's function to exhibit such an effect, where the propagation velocity of the light cone is determined by the maximal quasi-particle group velocity. In cases where quasi-particles are long lived, we expect to observe a "clean" light cone effect over a large time window. On the other hand, when there is a substantial decay rate, we expect the structure of the light cone to be modified. While it is more or less obvious that this intuition will hold for local quenches[121] it is a priori completely unclear whether it carries over to global ones. Closely related questions have been recently investigated for global quenches in the context of perturbed conformal field theories[122] as well as certain lattice models[123].

A. Non-interacting case

In order to set the stage we first consider quenches in the non-interacting case $U = 0$. We prepare the system in the density matrix $\rho_0(\beta,\delta_i)$ and, to keep things as simple as possible, time evolve with $H(0,\delta_f,0)$. We focus on the single particle Green's function (21). An example of the light cone effect is shown in Fig. 13. The real and imaginary parts of $\mathcal{G}(L/2+j, L/2, t)$ are seen to be very small outside a light cone that spreads with a velocity that equals the maximal group velocity of elementary excitations of the post-quench Hamiltonian. In the absence of interactions the structure of the light cone can be straightforwardly analyzed. For ease of presentation we restrict ourselves to odd separations j, choosing (even) $L/2$ as the reference point. For odd separations the Green's function is real, see Eq. (19) (even separations can be treated in complete analogy). In the thermodynamic limit our object of in-

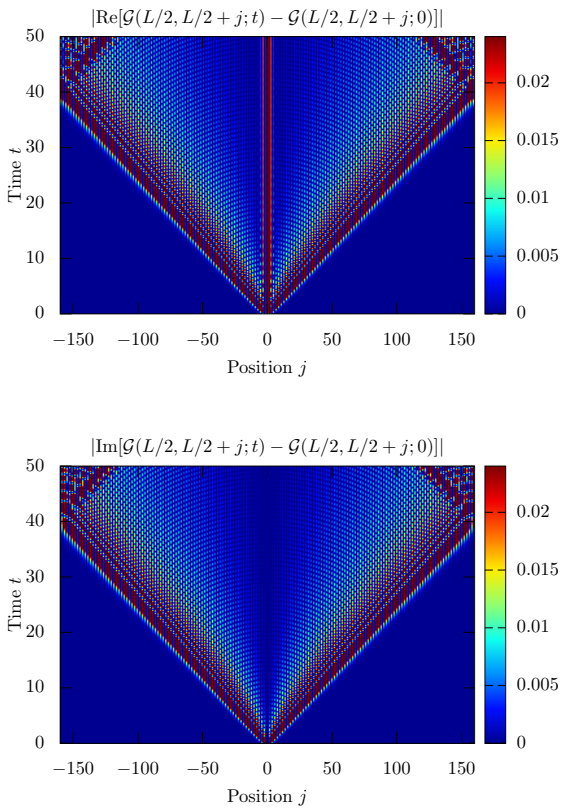

FIG. 13. Dynamics of the full Green's function $\mathcal{G}(L/2, L/2+j;t)$ as a function of time. The system is initialized in the density matrix $\rho_0(2, 0.5)$ and time evolved with the integrable (free) Hamiltonian $H(0,0,0)$. The light cone's edge is spreading with velocity $v_{\max} = 2\max_k \epsilon'_+(k)\big|_{J_2=0;\delta=0} = 2J_1$, see Eq. (11). The signal outside of the light cone decays exponentially in time.

terest $\mathfrak{g}(j,t) = \mathcal{G}(L/2, L/2+j;t)$ is thus given by

$$\mathfrak{g}(j,t) = \int_0^\pi \frac{\mathrm{d}k}{2\pi} e^{ikj - i\varphi_k(\delta_i)} \Big[n_{++}(k) - n_{--}(k) - n_{+-}(k) e^{i\epsilon_{+-}(k)t} + n_{-+}(k) e^{i\epsilon_{-+}(k)t} \Big]. \quad (44)$$

The contribution due to the n_{++} and n_{--} terms is time independent and plays no role in the light cone effect at large separations j. We now simplify the problem further by taking $\delta_f = 0$. The relevant part of the integral is then given by

$$\mathfrak{g}(j,t) \simeq \int_0^\pi \frac{\mathrm{d}k}{\pi} e^{ikj} \tilde{n}_{+-}(k) \cos\left(4t\cos k\right). \quad (45)$$

where we introduced

$$\tilde{n}_{+-}(k) = \frac{i}{2} \sin(\varphi_k(\delta_i)) \tanh\left(\frac{\beta}{2}\varepsilon_+^{(0)}(k)\right). \quad (46)$$

The structure of $\tilde{n}_{+-}(k)$ is such that there are no branch points in the complex k-plane. The only singularities are simple poles at positions determined by the argument of the tanh. Depending on the ratio j/t we have to distinguish between three regimes. It is convenient to define a parameter γ by

$$\gamma = \sqrt{\frac{\frac{\pi^2}{4\beta^2}+1}{1-\delta_i^2}} > 1. \quad (47)$$

1. *Interior of the light cone: $j < 2v_{\max}t$*

The first regime is characterized by $j < 2v_{\max}t$, where $v_{\max} = 2$ is the maximal group velocity of elementary excitations. As long as $2v_{\max}t$ is sufficiently larger than $j \gg 1$, the k-integral can be evaluated by a straightforward stationary phase approximation, which gives

$$\mathfrak{g}(j,t) \sim \frac{1}{2\sqrt{2\pi t}} \mathfrak{f}\left(\frac{j}{2v_{\max}t}\right) \times \mathrm{Im}\left[e^{i\left(\sqrt{(2v_{\max}t)^2 - j^2} + j\arcsin\left(\frac{j}{2v_{\max}t}\right) - \frac{\pi}{4}\right)}\right],$$
$$\mathfrak{f}(z) = \frac{z\delta_i \tanh\left(\beta\sqrt{1-(1-\delta_i^2)z^2}\right)}{\sqrt{1-(1-\delta_i^2)z^2}\ |1-z^2|^{1/4}}. \quad (48)$$

We see that inside the light cone the real part of the Green's function displays an oscillating power-law decay with exponent 3/2 (at late times).

2. *Short-time regime: $2v_{\max}t\gamma < j$*

In this regime the integrand features two saddle points in the complex k-plane at $k_\pm = \frac{\pi}{2} \pm i\mathrm{arccosh}\left(\frac{j}{2v_{\max}t}\right)$. When deforming the integration contour to pass through k_+, one encounters at least the simple pole at $k = \frac{\pi}{2} + i\mathrm{arccosh}(\gamma)$. The leading contribution to the integral stems from this pole. For large j we then obtain

$$\mathfrak{g}(j,t) \sim A(j) e^{-\left(j\ \mathrm{arccosh}(\gamma) - 2v_{\max}t\sqrt{\gamma^2-1}\right)},$$
$$A(j) = \frac{\delta_i \cos\left((j-1)\pi/2\right)}{2\beta(1-\delta_i^2)\sqrt{\gamma^2-1}}. \quad (49)$$

This shows an exponential increase in time.

3. *Intermediate regime: $j < 2v_{\max}t\gamma < j\gamma$.*

Interestingly there exists an intermediate regime that separates the interior of the light cone from the early time behaviour. For times $j < 2v_{\max}t\gamma < \gamma j$ and large values of j, the integral (45) can be evaluated by deforming the integration contour into the complex plane until it passes through the saddle point $k_+ = \frac{\pi}{2} + i\mathrm{arccosh}\left(\frac{j}{2v_{\max}t}\right)$. As long as $\mathrm{Im}(k_+)$ is smaller than the imaginary parts of the simple poles of the integrand, which defines the intermediate regime, the leading contribution to the integral (45)

can be obtained by a saddle point approximation. This gives

$$\mathfrak{g}(j,t) \sim \frac{(-1)^{\frac{(j-1)}{2}}}{4\sqrt{2\pi t}}\mathfrak{f}\left(\frac{j}{2v_{\max}t}\right) \times e^{-\left(j\,\mathrm{arccosh}\left(\frac{j}{2v_{\max}t}\right)-\sqrt{j^2-(2v_{\max}t)^2}\right)}. \quad (50)$$

Equation (50) provides a good approximation of the integral only "far enough" from the light cone $j = 2v_{\max}t$ (as it exhibits a singularity at $j = 2v_{\max}t$).

Fig. 14 reports a representative fixed-separation cut of $\mathcal{G}(0,j;t)$ (here we have used invariance under translations by two sites to shift the reference position to zero), comparing the expansions (48), (49), and (50) with the exact expression obtained by numerical integration of (45). The agreement is clearly excellent.

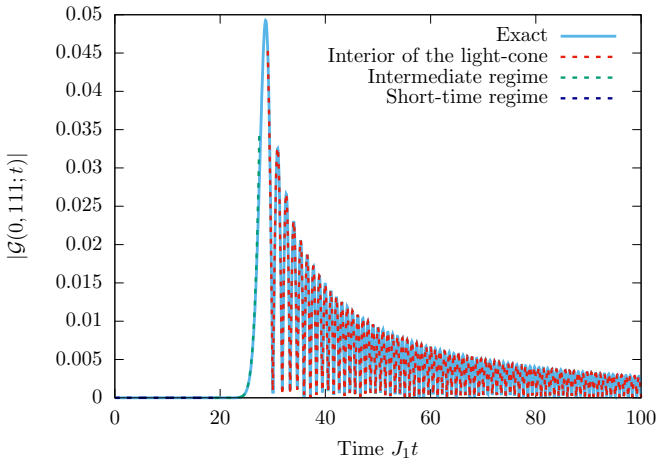

FIG. 14. Time evolution of $\mathcal{G}(0,111;t)$. The full line is obtained numerically integrating the exact expression (45), while the dashed lines are obtained using the asymptotic expansions (48), (49), (50).

4. *Proximity of the light cone*

For $\delta_f = 0$ we can furthermore describe the regime close to the light cone $j = 2v_{\max}t$. Starting from equation (45), we again deform the integration contour into the complex plane so that it passes through the saddle point at k_+. We then make the approximation that we can replace the factor $\widetilde{n}_{+-}(k)$ in the integrand by its value at the saddle point $\widetilde{n}_{+-}(k_+)$. Deforming the contour back to the real line we obtain the following approximation to the integral

$$\mathfrak{g}(j,t) \simeq \mathfrak{h}\left(\frac{j}{2v_{\max}t}\right)\mathrm{Im}\left[\int_0^\pi \frac{\mathrm{d}k}{\pi}\, e^{ikj+4ti\cos k}\right], \quad (51)$$

where

$$\mathfrak{h}(z) = \frac{z\delta_i}{2}\frac{\tanh\left(\beta\sqrt{1-(1-\delta_i^2)z^2}\right)}{\sqrt{1-(1-\delta_i^2)z^2}} \quad (52)$$

Carrying out the integral then gives

$$\mathfrak{g}(j,t) \simeq (-1)^{\frac{(j-1)}{2}}\,\mathfrak{h}\left(\frac{j}{2v_{\max}t}\right)J_j(4t). \quad (53)$$

As can be seen from Fig. 15, this is a very good approximation. For large j we can furthermore expand the Bessel function for large orders.[124] This allows us to recover the results of the stationary phase/saddle point approximations for the intermediate regions and the interior of the light cone. In the vicinity of the light cone, i.e. $2v_{\max} \approx j$, we find

$$\mathfrak{g}(j,t) \simeq \frac{(-1)^{\frac{(j-1)}{2}}}{2^{-1/3}j^{1/3}}\,\mathfrak{h}\left(\frac{j}{2v_{\max}t}\right)\mathrm{Ai}\left(\frac{j-2v_{\max}t}{2^{-1/3}j^{1/3}}\right). \quad (54)$$

As shown in Fig. 15 this provides a very good approximation of $\mathfrak{g}(j,t)$ close to the light cone. Similar results involving the Airy function have been previously obtained for the propagation of fronts in "inhomogeneous quantum quenches" in tight-binding and XX models.[125–127] The setting in these works is different in that the initial state features a step-like density profile, and the observable of interest is the time evolution of the density.

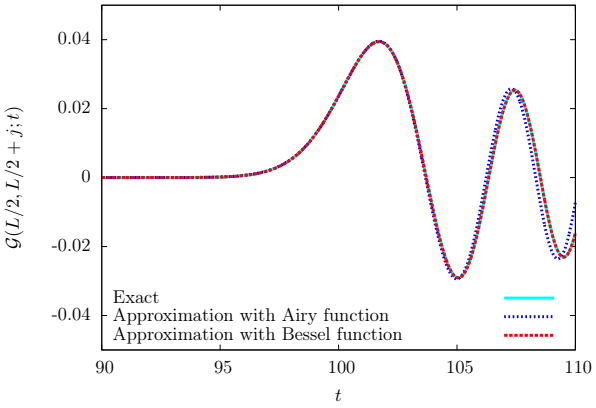

FIG. 15. Comparison of the Green's function $\mathcal{G}(0,j;t)$ for an infinite system as a function of time at fixed distance $j = 401$ with the approximations (53) and (54). The system is initialized in the density matrix $\rho_0(2, 0.5)$ and time evolved with the free Hamiltonian $H(0.5, 0, 0)$.

5. *"Width" of the light cone*

We are now in a position to define the width of the light cone. This is most conveniently done by considering the approximation (54). At large values of j most of the variation of $\mathfrak{g}(t,j)$ in the vicinity of the light cone is due to the Airy Function. Irrespective of the details of how one defined the width $\sigma(j)$, it then scales as

$$\sigma(j) \propto j^{1/3}. \quad (55)$$

This behaviour is the same as for the inhomogeneous quenches in lattice models[125–127], and was argued to hold for inhomogeneous quenches in perturbed conformal field theories as well[128].

6. $\delta_f \neq 0$ *case*

When the final dimerization is non-zero the analytic structure of the integrand in (44) becomes more complicated: $\epsilon_{+-}(k)$ has branch cuts in the complex k-plane. In addition, the number of saddle points increases. This complicates the analysis of the short-time regime. Nonetheless, the behaviour of the Green's function in the intermediate regime, $Cj < 2v_{\max}t < j$ ($C < 1$), and in the interior of the light cone, $2v_{\max}t > j$, can be determined as above. The structure remains very similar: for $2v_{\max}t > j$ the Green's function decays as $t^{-\frac{3}{2}}$ and for $Cj < 2v_{\max}t < j$ it decays exponentially, but there are oscillatory contributions multiplying the exponential decay. Importantly, the "width" $\sigma(j)$ of the light cone scales always as $j^{1/3}$.

B. Interacting case

The structure of the light cone in the interacting case remains qualitatively similar, see Fig. 16. The most marked difference is that the height of the maximum at fixed separation now displays a much faster decay in j as is shown in Fig. 17.

In order to determine the width of the light cone we fit the Green's function in the vicinity of the light cone by an expression of the form

$$\mathcal{G}(L/2, L/2+j, t) = a\mathrm{Ai}\left(b(2v_{\max}t - j)\right) , \qquad (56)$$

where a, b and $v_{\max}$ are fit parameters (a and b are j-dependent). This provides an excellent description in the proximity of the light cone for a wide range of j as is shown for an example in Fig. 18. The width $\sigma(j)$ of the light cone can be extracted from the j-dependence of the parameter b, and we find that

$$\sigma(j) \propto j^{\alpha} \qquad \alpha < 1 . \qquad (57)$$

The main difficulty we face is that we can only reach separations of around 160 sites, which imposes serious limitations to the precision with which we can determine the scaling exponent α. In the non-interacting case we need to consider extremely large values of j to observe the scaling $\sigma(j) \propto j^{1/3}$. Comparing the scaling in the free and interacting case for different values of U in the regime accessible to us, we do not find a significant dependence of the scaling exponent on the interaction strength U, and all of our results are compatible with an exponent $\alpha = 1/3$, see Fig. 19. We have also considered some quenches with $\delta_f > 0$ and come to identical conclusions.

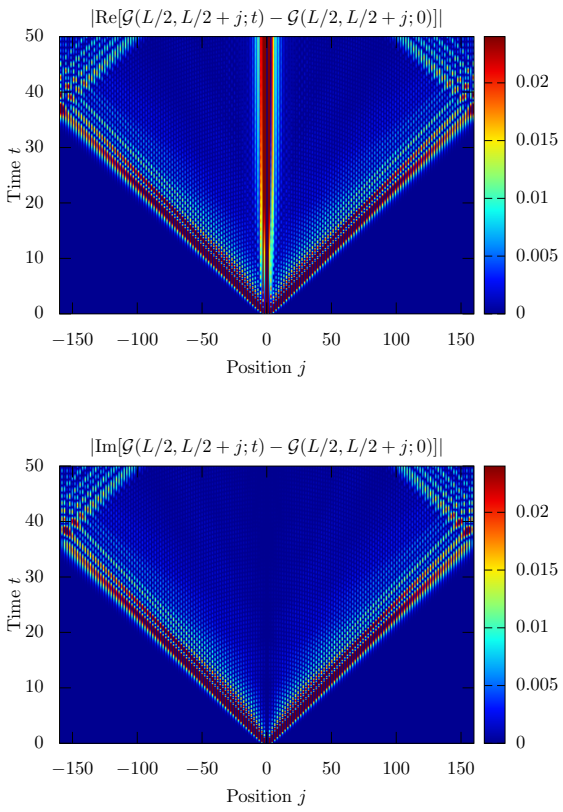

FIG. 16. Dynamics of the full Green's function $\mathcal{G}(L/2, L/2+j; t)$ as a function of time. The system is initialized in the density matrix $\rho_0(2, 0.5)$ and time evolved with the non-integrable Hamiltonian $H(0.5, 0, 0.4)$. The signal outside of the light cone decays exponentially in time.

VII. QUANTUM BOLTZMANN EQUATION

An important question is whether the set (34) of coupled integro-differential equations can be simplified for late times by removing the time integration, in analogy with standard quantum Boltzmann equations (QBE).[90,94] Given that the structure of (34) is rather different to the standard QBE case, *cf.* Ref. [90], it is not *a priori* clear that this is possible. More precisely, as (34) includes an $\mathcal{O}(U)$ term intimately related to the existence of a PT plateau, it is far from obvious that the solutions of the EOM will only depend on t through the rescaled variables $\tau = U^2 t$ at late times, as is the case in the standard QBE framework.[90,94]

A. Simplifying the EOM

In all the cases that we have analyzed, the "off-diagonal" two-point functions $n_{\mu\bar{\mu}}(k; t)$ become negligible at sufficiently late times and small values of U, see Figs. 20–22 for representative examples. This leads us to

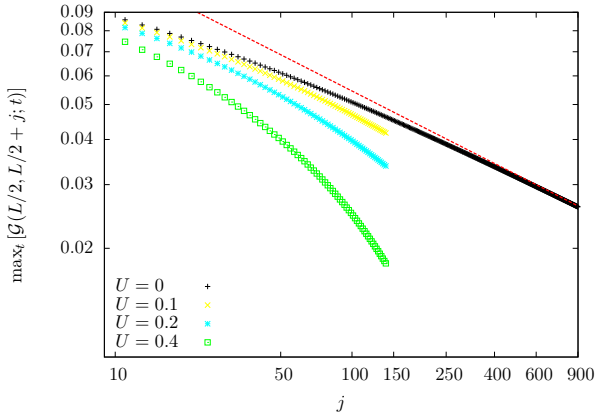

FIG. 17. Double logarithm plot of $\max_t \mathcal{G}(L/2, L/2+j;t)$ as a function of the odd separation j, for a system of length $L = 1920$ ($U = 0$) and $L = 320$ ($U \neq 0$), initialized in the state $\rho_0(2, 0.5)$ and evolved with $H(0.5, 0, U)$ for $U = 0, 0.1, 0.2, 0.4$. Different symbols correspond to different values of the interaction and the red dashed line is $\propto j^{-1/3}$.

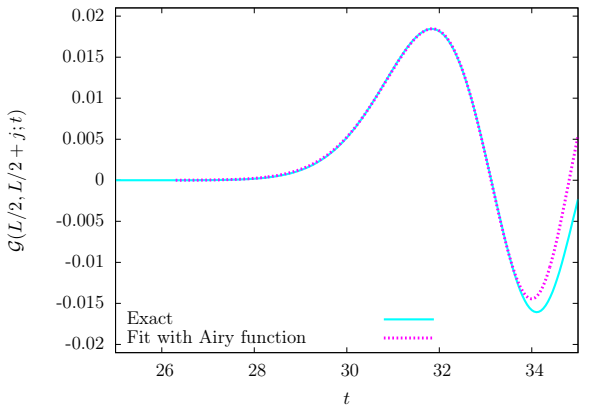

FIG. 18. Airy Function fit of the Green's function $\mathcal{G}(L/2, L/2+j;t)$ as a function of time at fixed distance $j = 137$. The system is initialized in the density matrix $\rho_0(2, 0.5)$ and time evolved with the non-integrable Hamiltonian $H(0.5, 0, 0.4)$.

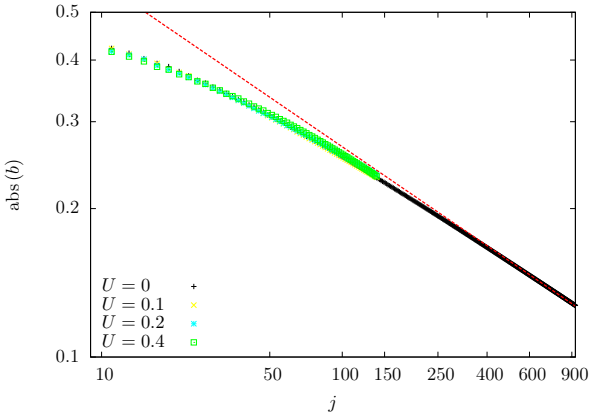

FIG. 19. Double logarithm plot of the fitting parameter b (*cf.* Eq. (56)) as a function of j. The system, of length $L = 1920$ for $U = 0$ and $L = 320$ for $U \neq 0$, is initialized in the density matrix $\rho_0(2, 0.5)$ and time evolved with the non-integrable Hamiltonian $H(0.5, 0, U)$ with $U = 0, 0.1, 0.2, 0.4$. Different symbols correspond to different values of U and the red dashed line is $\propto j^{-1/3}$.

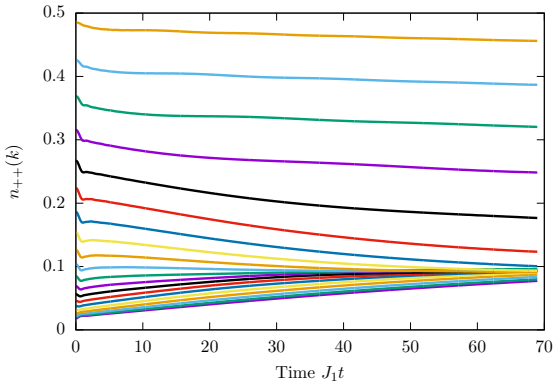

FIG. 20. The time dependence of the Bogoliubov mode occupation numbers $n_{++}(k)$ for a system of size $L = 320$ initialized in the density matrix $\rho(2, 0.5)$ and time evolved with $H(0.375, 0, 0.4)$. The different lines are different k-modes (we restrict our attention to $0 \leq k \leq \pi/2$, as $n_{\mu\nu}(k,t) = \mu\nu n_{\mu\nu}(\pi - k, t)$, and plot every fourth k-mode).

formulate the following approximation

$$n_{\mu\bar{\mu}}(k,t) \approx 0 \qquad \text{for } t \gg U^{-1} \,, \tag{58}$$

where we have introduced the notations $\bar{\mu} = -\mu$. We note that our approximation is consistent with relaxation of $n_{\mu\nu}(k,t)$ towards their thermal values at late times as this would suggest $n_{\mu\bar{\mu}}(k;\infty) \sim \mathcal{O}(U)$ and $n_{\mu\mu}(k;\infty) \sim \mathcal{O}(U^0)$.

We now use the approximation (58) to simplify the EOM. We drop the equation for $n_{+-}(k,t)$ and retain only those for $n_{++}(k,t)$ and $n_{--}(k,t)$. These do not contain $\mathcal{O}(U^0)$ contributions on the right-hand side of (34), but they do feature $\mathcal{O}(U^1)$ terms, which can be cast in the form

$$8U\mathrm{Im}\left\{\left[A_{\bar{\mu}}(k) + B_{\bar{\mu}}(k,t)\right] n_{\mu\bar{\mu}}(k) e^{i\epsilon_{\mu\bar{\mu}}(k)t}\right\} \,, \tag{59}$$

where we have introduced notations

$$A_\mu(k) \equiv \sum_\gamma \sum_{q>0} V_{\bar{\mu}\gamma\gamma\mu}(k,q,q,k) n_{\gamma\gamma}(q) \,, \tag{60}$$

$$B_\mu(k,t) \equiv \sum_\gamma \sum_{q>0} V_{\bar{\mu}\gamma\bar{\gamma}\mu}(k,q,q,k) n_{\gamma\bar{\gamma}}(q) e^{i\epsilon_{\gamma\bar{\gamma}}(q)t} \,. \tag{61}$$

The function $B_\mu(k,t)$ sums an oscillating phase multiplied by a smooth function and consequently decays to zero at late times (see below). $A_\mu(k)$, however, is independent of time and its presence generally complicates

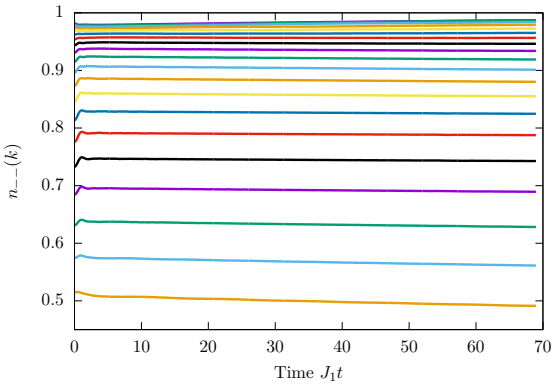

FIG. 21. Same as Fig. 20 for $n_{--}(k)$.

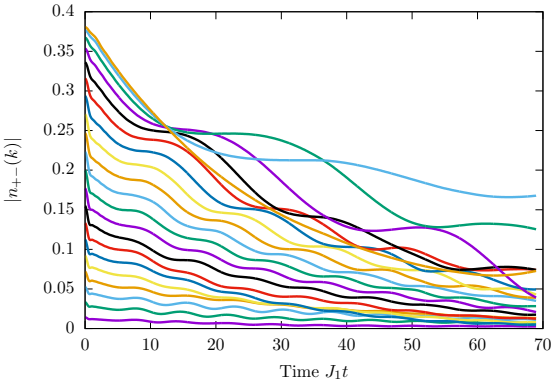

FIG. 22. Same as Fig. 20 for $|n_{+-}(k)|$.

our analysis of the long time limit. An exception occurs for the special value $\delta_f = 0$, where

$$V_{\eta\gamma\gamma\bar{\eta}}(k,q,q,k)|_{\delta_f=0} = 0 \quad \forall \eta,\gamma\,,\forall k,q\,, \tag{62}$$

and concomitantly $A_\mu(k)$ vanishes. For the rest of the section we will focus on this special case, and show that the remaining $\mathcal{O}(U)$ terms do not contribute in the "Boltzmann scaling limit"

$$U \to 0 \quad \text{and} \quad t \to \infty \quad \text{with} \quad \tau = tU^2 \quad \text{fixed}\,. \tag{63}$$

This then implies that we may use a QBE description at late times. We return to the general case $\delta_f \neq 0$ in Sec. VII E.

B. QBE for $\delta_f = 0$

In the scaling limit (63), the diagonal EOM (34) for $\delta_f = 0$ become

$$\partial_\tau n_{\mu\mu}(k,\tau) = \lim_{sc} 4iU^{-1}\left(B_\mu(k,t)n_{\bar{\mu}\mu}(k)e^{i\epsilon_{\bar{\mu}\mu}(k)t} + \text{c.c.}\right) + \lim_{sc}\sum_{\boldsymbol{p}>0,\boldsymbol{\nu}}\int_0^t \mathrm{d}s\; e^{iE_{\boldsymbol{\nu}}(\boldsymbol{p})(t-s)}F^\mu_{\boldsymbol{\nu}}(\boldsymbol{p};k;s)\,. \tag{64}$$

Here $\lim_{sc}$ denotes the Boltzmann scaling limit (63) and we have collected the integrand of the s-integral into a single function $F^\mu_{\boldsymbol{\nu}}(\boldsymbol{p};k;s)$ to lighten notations. At late times in the scaling limit (63) the $B_\mu(k,t)$-term can be evaluated by a stationary phase approximation

$$\begin{aligned}&\lim_{sc}\frac{4i}{U}B_\mu(k,t)n_{\bar{\mu}\mu}(k)e^{i\epsilon_{\bar{\mu}\mu}(k)t}\\ &= \lim_{sc}\frac{U}{\tau^{3/2}}\sin\left(\frac{\tau\epsilon_{+-}(0)}{U^2}-\frac{\pi}{4}\right)\mathcal{V}_\mu(k)e^{i\epsilon_{\bar{\mu}\mu}(k)\tau U^{-2}}\\ &= 0\,.\end{aligned} \tag{65}$$

Here $\mathcal{V}_\mu(k)$ is an amplitude depending on the initial state and the vertex function

$$\mathcal{V}_\mu(k) = \frac{2\mu\delta_i\sin(k)n_{\bar{\mu}\mu}(k)}{\sqrt{2\pi}(\epsilon''_{+-}(0))^{3/2}}\frac{|\cos(k)|}{\cos(k)}\tanh(\beta_i)\,. \tag{66}$$

The exponent 3/2 in (65) is a consequence of $n_{+-}(k,0)$ being zero at the saddle point $k=0$, *cf.* Eq. (24). From Eq. (65), we conclude that the $\mathcal{O}(U)$ terms do not contribute in the scaling limit when $\delta_f = 0$.

This leaves us with the $\mathcal{O}(U^2)$ contribution on the right-hand side of Eq. (64). According to our basic approximation (58), this can be simplified in the long time limit because the off-diagonal two point functions $n_{+-}(k;s)$ can be neglected for $s \gg U^{-1}$. We now make the further assumption that the diagonal mode occupation numbers $n_{\mu\mu}(k;s)$ depend on s only through sU^2, *i.e.* they are very slowly varying. This assumption is again motivated by numerical results obtained by integrating the full EOM, see Figs. 20 and 21 for a representative example. The $\mathcal{O}(U^2)$ terms can then be treated as follows. We introduce an intermediate timescale $U^{-1} \ll \bar{t} \ll t$ and split the time integral into two parts

$$\begin{aligned}&\int_0^t \mathrm{d}s\; e^{iE_{\boldsymbol{\nu}}(\boldsymbol{p})(t-s)}F^\mu_{\boldsymbol{\nu}}(\boldsymbol{p};k;s)\\ &\quad= \int_0^{\bar{t}} \mathrm{d}s\; e^{iE_{\boldsymbol{\nu}}(\boldsymbol{p})(t-s)}F^\mu_{\boldsymbol{\nu}}(\boldsymbol{p};k;s)\\ &\qquad+\int_0^{t-\bar{t}} \mathrm{d}s\; e^{iE_{\boldsymbol{\nu}}(\boldsymbol{p})s}F^\mu_{\boldsymbol{\nu}}(\boldsymbol{p};k;t-s)\,.\end{aligned} \tag{67}$$

We then make the assumption that the first term on the right hand side of (67) does not contribute in our scaling limit, while the remaining integral can be treated as follows. We first replace $F^\mu_{\boldsymbol{\nu}}(\boldsymbol{p};k;s)$ by its smooth part $F^\mu_{\boldsymbol{\nu}}(\boldsymbol{p};k;s)_{\text{slow}}$ depending on s only through $U^2 s$, this is motivated by numerical analysis as discussed above. We then add an infinitesimal convergence factor $i\eta$, to $E_{\boldsymbol{\nu}}(\boldsymbol{p})$ in the exponential factor of the integrand in order to ensure the convergence of the integral. In principle the parameter η should be taken to zero after the Boltzmann scaling limit has been performed. In practice we keep η small but finite and ensure that our results for the Green's function only depend very weakly on it in the time interval considered. This procedure is equivalent to

the regularization adopted in Refs. [101, 129]. Next we expand the function $F^{\mu}_{\boldsymbol{\nu}}(\boldsymbol{p};k;t-s)_{\rm slow}$ around t, which gives

$$\int_0^{t-\bar{t}} \mathrm{d}s\; e^{i(E_{\boldsymbol{\nu}}(\boldsymbol{p})+i\eta)s} F^{\mu}_{\boldsymbol{\nu}}(\boldsymbol{p};k;t-s)_{\rm slow} = \\ = \sum_{n=0}^{\infty} \frac{(-1)^n}{n!} \frac{\mathrm{d}^n}{\mathrm{d}s^n} F^{\mu}_{\boldsymbol{\nu}}(\boldsymbol{p};k;t)_{\rm slow} \int_0^{t-\bar{t}} \mathrm{d}s\; e^{i(E_{\boldsymbol{\nu}}(\boldsymbol{p})+i\eta)s} s^n \; . \tag{68}$$

As $F^{\mu}_{\boldsymbol{\nu}}(\boldsymbol{p};k;s)_{\rm slow}$ is a function of $U^2 s$ its derivatives are suppressed by factors of U^2 in the Boltzmann scaling limit, which implies that we only need to retain the first contribution. Evaluating the first integral we have

$$\lim_{sc} \int_0^{t-\bar{t}} \mathrm{d}s\; e^{i[E_{\boldsymbol{\nu}}(\boldsymbol{p})+i\eta](t-s)} = \frac{i}{E_{\boldsymbol{\nu}}(\boldsymbol{p})+i\eta} \equiv D(E_{\boldsymbol{\nu}}(\boldsymbol{p})) \; . \tag{69}$$

Putting everything together we arrive at a QBE for the mode occupation numbers

$$\partial_\tau n_{\mu\mu}(k,\tau) = -\sum_{\gamma,\eta} \sum_{p,q>0} \widetilde{K}^{\gamma\eta}_{\mu}(p,q|k) n_{\gamma\gamma}(p,\tau) n_{\eta\eta}(q,\tau) \\ - \sum_{\gamma,\eta,\epsilon} \sum_{p,q,r>0} \widetilde{L}^{\gamma\eta\epsilon}_{\mu}(p,q,r|k) n_{\gamma\gamma}(p,\tau) \\ \times n_{\eta\eta}(q,\tau) n_{\epsilon\epsilon}(r,\tau) \; . \tag{70}$$

Here the kernels are given by

$$\widetilde{K}^{\gamma_1\gamma_2}_{\alpha}(k_1,k_2|q) = 4 \sum_{k_3,k_4>0} \sum_{\nu,\nu'} \widetilde{X}^{\gamma_1\gamma_2\nu\nu'|\nu\nu'\gamma_2\gamma_1}_{\boldsymbol{k}|\boldsymbol{k}'}(\alpha|q), \\ \widetilde{L}^{\gamma_1\gamma_2\gamma_3}_{\alpha}(k_1,k_2,k_3|q) = 8 \sum_{\nu} \sum_{k_4>0} \widetilde{X}^{\gamma_1\gamma_2\gamma_3\nu|\nu\gamma_3\gamma_2\gamma_1}_{\boldsymbol{k}|\boldsymbol{k}'}(\alpha|q) \\ -16 \sum_{\nu} \widetilde{X}^{\gamma_1\gamma_2\nu\gamma_2|\gamma_3\nu\gamma_3\gamma_1}_{k_1k_2k_1k_2|k_3k_1k_3k_1}(\alpha|q), \\ \widetilde{X}^{\boldsymbol{\gamma}|\boldsymbol{\alpha}}_{\boldsymbol{k}|\boldsymbol{q}}(\alpha|q) = Y^{\boldsymbol{\gamma}}_{\alpha\alpha}(\boldsymbol{k},q) V_{\boldsymbol{\alpha}}(\boldsymbol{q}) D(E_{\boldsymbol{\gamma}}(\boldsymbol{k})) \\ -(\boldsymbol{\gamma},\boldsymbol{k}) \leftrightarrow (\boldsymbol{\alpha},\boldsymbol{q}) \; . \tag{71}$$

The Boltzmann equation has been derived in the scaling limit (63). In practice, this limit cannot be accessed in numerical computations starting from $t=0$. Instead, we keep U small but *finite* and initialize the QBE at a *finite* time $t_0 \gg U^{-1}$ using the occupation numbers computed up to $t=t_0$ with the full EOM (34).

In Figs. 23 we present results obtained using the QBE for cases where the system is initialized in the density matrix $\rho_0(2,0.5)$ and time evolved with $H(J_2,0,0.4)$, where $J_2 = 0.375, 0.5$. The QBE is initialized at time $t_0 = 20$. Even for the relatively large value of $U=0.4$, we see that the results of the QBE are in good quantitative agreement with the full EOM. The agreement worsens for larger separations, which is not surprising as the Green's function itself becomes smaller. At late times the mode occupation numbers also approach their thermal values.

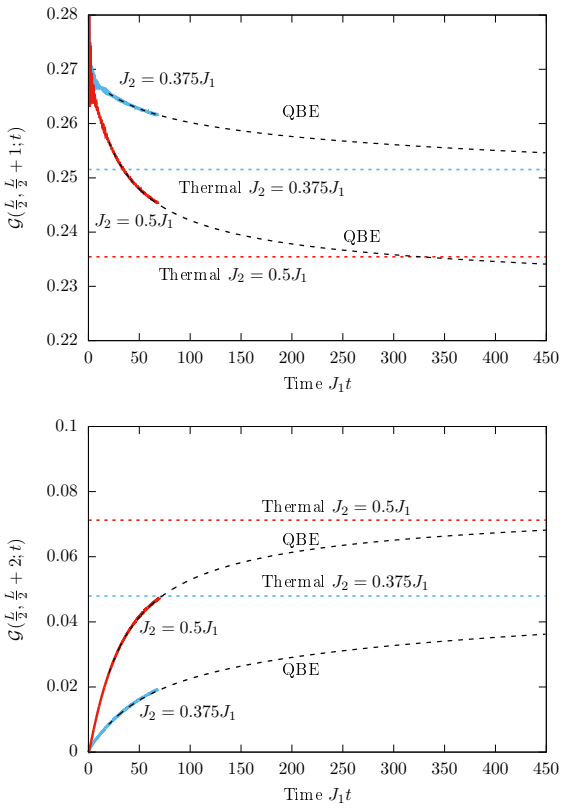

FIG. 23. $\mathcal{G}(L/2, L/2+j;t)$ with (upper) $j=1$ and (lower) $j=2$ for a system of size $L=320$ initially prepared in a state with density matrix $\rho(2,0.5)$, and time evolved with $H(J_2,0,0.4)$. Full lines show results obtained by integrating the EOM (34), and black dashed lines indicate the QBE results.

This approach should not be taken too literally as we now explain. The non-interacting Fermi-Dirac distribution (for arbitrary β and μ) is always a stationary solution of the QBEs (70). It is believed that for non-integrable models it is the only stationary solution.[101] If this holds true, the value to which a mode occupation number relaxes is determined by the number density and the kinetic energy at the time the QBE is initialized.[94,129] This means that in the late time limit we expect the QBE to converge to values that agree with the "correct" thermal values only up to corrections of order $\mathcal{O}(U)$.

C. Scaling form of the Green's function

In the QBE framework the Green's function depends on U both via the rescaled time τ, and through the initial conditions imposed at time t_0. We express this as

$$\mathcal{G}(i,j;t,U) = \mathcal{F}_{ij}(\tau,U) \; , \qquad t > t_0 \gg U^{-1} \; . \tag{72}$$

Expanding $\mathcal{F}_{ij}(\tau,U)$ to leading order in U (at fixed τ) then gives

$$\mathcal{F}_{ij}(\tau,U) \sim \mathcal{F}_{ij}(\tau,0) + \mathcal{O}(U) \; . \tag{73}$$

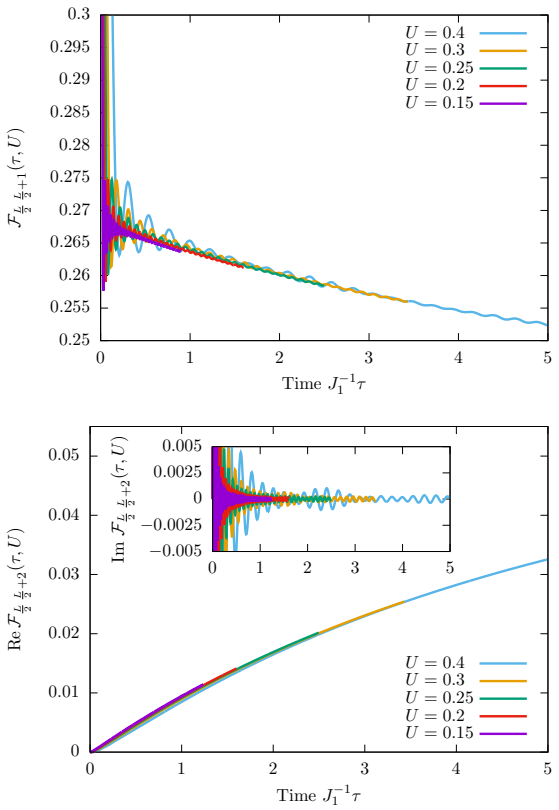

FIG. 24. Green's functions $\mathcal{F}_{L/2\,L/2+1}(\tau, U)$ (top) and $\mathcal{F}_{L/2\,L/2+2}(\tau, U)$ (bottom) obtained by numerical solution of the full EOM (34) for a system prepared in the state with density matrix $\rho_0(2, 0.5)$ and time evolved with $H(0.5, 0, U)$. Results for several values of U are plotted against the rescaled variable $\tau = U^2 t$.

We expect that the full EOM will give rise to the scaling form (72), (73) at sufficiently late times. This is indeed the case as shown in Fig. 24 for a representative example.

By virtue of its simpler structure, the QBE allows us to determine how the exponent (41) scales with the interaction strength U. To that end we consider the exponential fit (41) that we have found to give a good account of the intermediate time behaviour of the Green's function. Expanding the inverse relaxation time in powers of U

$$\tau_{ij}^{-1}(U) = \sum_{i=0}^{\infty} a_i U^i \,, \tag{74}$$

we have

$$\mathcal{G}(i,j;t;U) \approx \mathcal{G}(i,j)_{\mathrm{th}} + A_{ij}(J_2, 0, U) e^{-t a_0 - tU a_1 - \tau a_2} + \ldots \tag{75}$$

In order for this to be compatible with (72) we must have $a_0 = a_1 = 0$, $a_2 \neq 0$, which gives

$$\tau_{ij}^{-1}(J_2, \delta_f = 0, U) = U^2 a_2 + O(U^3) \,. \tag{76}$$

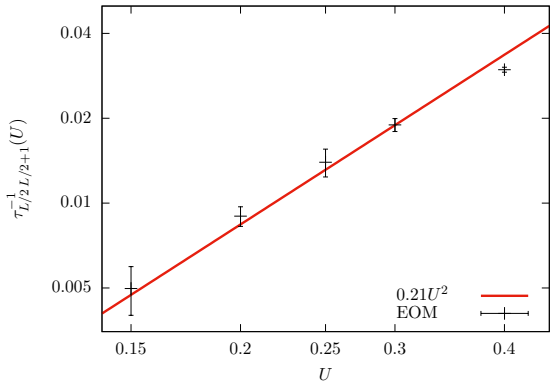

FIG. 25. Double logarithmic plot of the U-dependence of the inverse relaxation times $\tau^{-1}_{L/2\,L/2+1}(U)$ for a system initialized in the density matrix $\rho_0(2, 0.5)$ and time evolved with $H(0.5, 0, U)$. Relaxation times are obtained by fitting the EOM results to the form (41). Errors are estimated by varying the initial time at which the exponential fit is applied.

As shown in Fig. 25 for a particular example, the U^2-scaling in (76) is in good agreement with inverse relaxation times extracted from the numerical solution of the EOM.

We note that the scaling of inverse relaxation times with U found here differs from that obtained in Ref. [85]. In contrast to our quench protocol, Ref. [85] considers situations where the energy density in the initial state is $\mathcal{O}(U)$, which results in a U^4 scaling.

D. Mode occupation numbers

In order to obtain further indicators that integrability breaking perturbations lead to thermalization, we turn our attention to the (Bogoliubov) mode occupation numbers $n_{\mu\mu}(q, t)$ themselves. The first question to consider is whether we expect these quantities to relax at all? The number operators are local in momentum space, and hence are non-local in real space. It is then *a priori* unclear whether they will relax at late times (see, however, Ref. [130]). Here we take a practical point of view: we simply follow the evolution of $n_{\mu\mu}(k, t)$ on the time scales accessible to us, and compare them to the appropriate thermal values $n_{\mu\mu}(k, \beta_{\mathrm{eff}}, \mu_{\mathrm{eff}})$ of the putative stationary behaviour. The latter are calculated by standard second order perturbation theory in U; details are given in Appendix B.

In Fig. 26 we show results for the mode occupation numbers $n_{\mu\mu}(k, t)$ at several different times for a system of size $L = 320$ that has been prepared in the density matrix $\rho(2, 0, 0.5, 0)$ and evolved with $H(0.375, 0, 0.4)$ (see also the example reported in Ref. [75]). For short and intermediate times $J_1 t \lesssim 70$ we use the full EOM, while later times are analyzed in the framework of the QBE. The QBE is initialized at time $t_0 = 20$, and is in good

agreement with the full EOM until the latest times accessible by the latter. We observe that the mode occupation numbers slowly evolve towards the values for a system at thermal equilibrium with the correct particle and energy densities, see Appendix B. In particular, at the latest time reached ($t = 450$), the occupation numbers $n_{++}(k,t)$ are close to the appropriate thermal distribution. We recall that integration of the full EOM (34) indicates that the "off-diagonal" occupation numbers $n_{+-}(k,t)$ approach their thermal value (zero) in an oscillatory fashion, see Fig. 22. These results suggest that *the weak integrability breaking term induces thermalization of the system.*

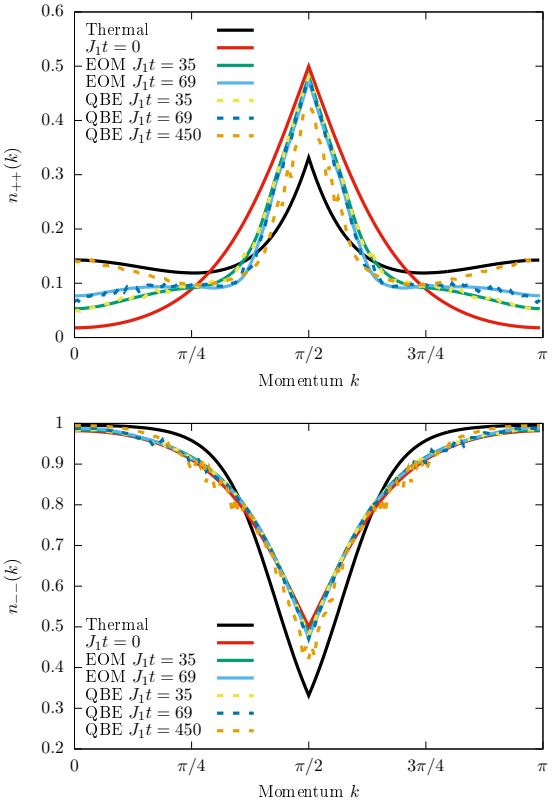

FIG. 26. Mode occupation numbers $n_{++}(k,t)$ (top) and $n_{--}(k,t)$ (bottom) for a system of size $L = 320$ that is initialized in the thermal state $\rho_0(2, 0.5)$ and time evolved with $H(0.375, 0, 0.4)$. Solid (dotted) lines are obtained by integrating the EOM (QBE). The solid black line is the thermal value found by means of second order perturbation theory in U.

E. Quantum Boltzmann equation for $\delta_f \neq 0$

In the case $\delta_f \neq 0$ we again observe that the off-diagonal two-point functions $n_{+-}(k,t)$ become $\mathcal{O}(U)$ at sufficiently late times; for $Jt \sim 100$ they are oscillating around the thermal value, found by means of second order perturbation theory. However, this fact can no longer be exploited in a straightforward manner to obtain a closed system of equations for the mode occupation numbers $n_{\mu\mu}(k,t)$. This is because for $\delta_f \neq 0$ the right hand side of the EOM (34) for the diagonal components contains a term which does not decay in time

$$8U \ \mathrm{Im}\left[A_{\bar{\mu}}(k) n_{\mu\bar{\mu}}(k,0) e^{i\epsilon_{\mu\bar{\mu}}(k)t}\right] . \tag{77}$$

Here $A_\mu(k)$ has been introduced in (60).

In spite of this, local observables computed from our numerical solutions of the EOM exhibit an approximate scaling collapse at sufficiently late times as is shown in Fig. 27 for two representative examples. This in turn allows us to repeat the arguments of the previous subsection for generic δ_f, and suggests that the inverse decay times scale as

$$\tau_{ij}^{-1}(J_2, \delta_f, U) \propto U^2. \tag{78}$$

In other words, *the time scale for thermalization is proportional to U^{-2} for generic δ_f.* This is consistent with our solution of the full EOM on the accessible time scales, *cf.* Fig. 28.

In order to obtain a quantum Boltzmann like equation for $\delta_f \neq 0$ we proceed as follows. The numerical solutions

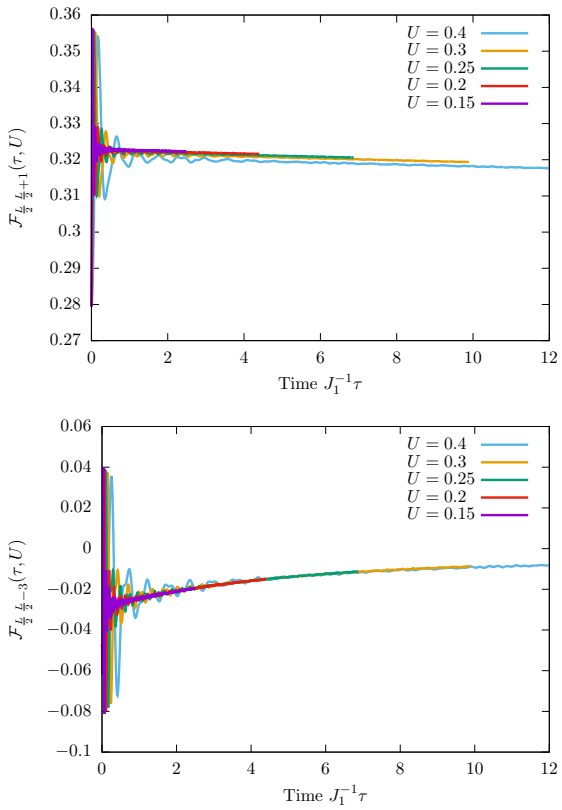

FIG. 27. (upper) $\mathcal{F}_{L/2\,L/2+1}(\tau, U) = \mathcal{G}(L/2, L/2+1; t, U)$ and (lower) $\mathcal{F}_{L/2\,L/2-3}(\tau, U) = \mathcal{G}(L/2, L/2-3; t, U)$, the system is initially prepared in the state $\rho_0(2, 0)$ and evolved with the Hamiltonian $H(0.5, 0.4, U)$, for different values of U. The time evolution is obtained by numerical solution of the full EOM (34) and plotted as a function of the rescaled variable $\tau = U^2 t$.

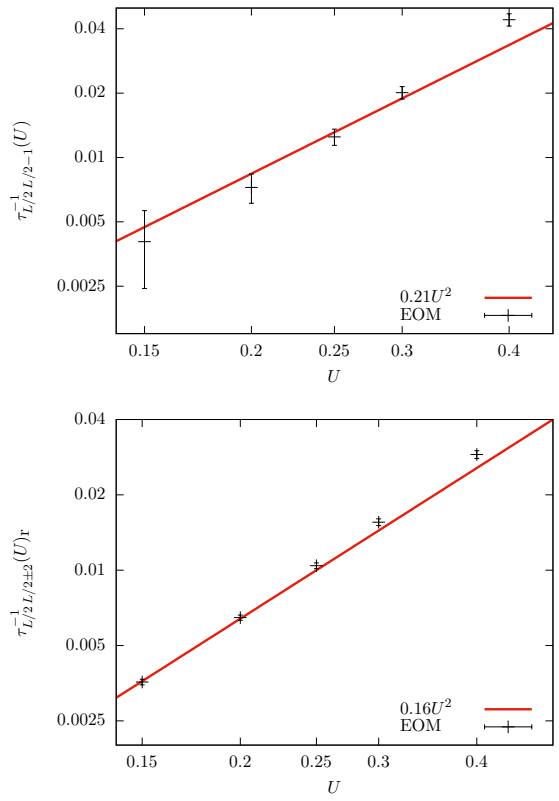

FIG. 28. The U dependence of the exponents (upper) $\tau^{-1}_{L/2\,L/2-1}(U)$ and (lower) $\tau^{-1}_{L/2\,L/2+2}(U)_{\rm r}$ obtained from the exponential fit (41), plotted in logarithmic scale.[107] In the lower panel the error bars are contained within the symbols. Data is presented for the time-evolution from the initial state $\rho_0(2,0)$ with Hamiltonian $H(0.5,0.1,U)$ for $U = 0.15, 0.2, 0.25, 0.3, 0.4$ (see also Figs. 27). The errors are estimated by varying the initial time at which the exponential fit is applied.

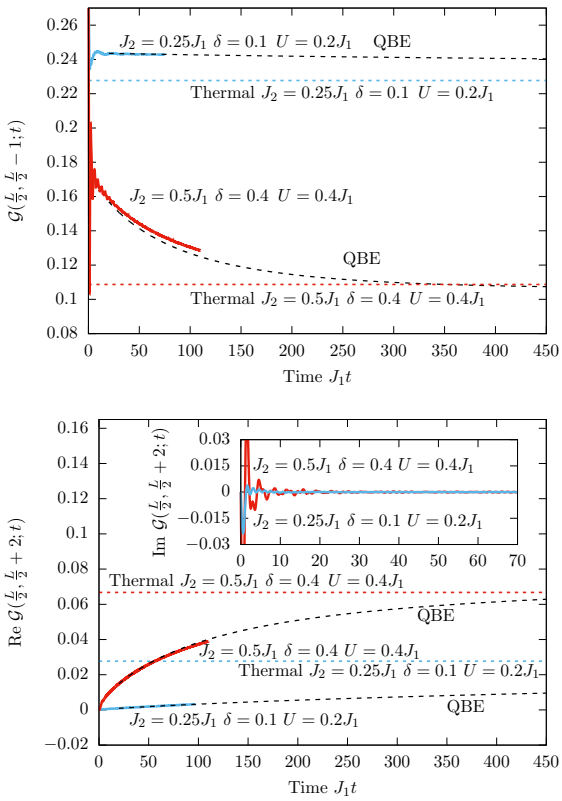

FIG. 29. $\mathcal{G}(L/2, L/2-1;t)$ (upper panel) and $\mathcal{G}(L/2, L/2+2;t)$ (lower panel) for two systems with Hamiltonians $H(0.25,0.1,0.2)$, $H(0.5,0.4,0.4)$ and size $L = 320$ initially prepared in a thermal state (14) with density matrix $\rho_0(2,0)$. The full lines are obtained by integrating the EOM (34) and the black dashed lines are found by means of the QBE.

of the full EOM indicate that the mode occupation numbers exhibit small amplitude, high-frequency oscillations on top of a smoothly varying part. Separating these two components using a low pass filter $\mathcal{L}$ we have

$$\begin{aligned} n_{\mu\mu}(k,t) &= \mathcal{L}[n_{\mu\mu}(k,t)] + (1-\mathcal{L})[n_{\mu\mu}(k,t)], \\ &= s_\mu(k,U^2t) + \Delta_\mu(k,t). \end{aligned} \tag{79}$$

The low-pass filter $\mathcal{L}$ separates the slowly varying contributions $s_\mu(k,U^2t)$ from the rapidly oscillating (small amplitude) parts $\Delta_\mu(k,t)$. We expect that the late time behaviour of local observables will not depend on the oscillatory parts. This expectation is based on the observation that a stationary phase approximation applied to the momentum sum would show that these contributions are suppressed, *cf.* Eq (21). Applying the low-pass filter $\mathcal{L}$ to the equation of motion (34), where the off-diagonal two-point functions n_{+-} have been neglected, and considering the Boltzmann limit (63), we find that $s_\mu(k,\tau)$ *satisfy the Boltzmann equation (70) with* $n_{\mu\mu}(k,\tau) \to s_\mu(k,\tau)$. Further details are presented in Appendix C. In Fig. 29 we show comparisons between results obtained from the quantum Boltzmann equation (70) for $s_\mu(k,t)$ to the full EOM (34). We see that the agreement is quite satisfactory, which gives us some confidence in the above line of argument.

To conclude our discussion of the $\delta_f \neq 0$ case, we note that the occupation numbers $s_\mu(k,\tau)$ appear to approach their thermal values (computed by second order perturbation theory) in the long time limit.

VIII. BREAKING THE U(1) SYMMETRY

One of the key features of the class of models (1) is that they possess a global U(1) symmetry associated with particle number conservation, see Sec. II. We expect PT to be robust with respect to breaking this symmetry. To check whether this is indeed the case we have investigated

quantum quenches to the class of models

$$\mathcal{H}(\gamma,h,U)=\frac{J}{2}\sum_i\left[c_i^\dagger c_{i+1}+\gamma c_i^\dagger c_{i+1}^\dagger+\text{h.c.}\right]+Jh\sum_i c_i^\dagger c_i+U\sum_i c_i^\dagger c_i c_{i+1}^\dagger c_{i+1}\,, \quad (80)$$

which are related to the Heisenberg XYZ chain in a magnetic field by a Jordan-Wigner transformation. The model (80) becomes integrable in several limits

1. For $U=0$ the model is non-interacting;
2. For $\gamma=0$ it is equivalent to the spin-1/2 Heisenberg XXZ chain in an external magnetic field;
3. For $h=-U$, where it is equivalent to the spin-1/2 Heisenberg XYZ chain.

In order to apply the EOM formalism we prepare the system in an initial density matrix with respect to which Wick's theorem holds. Our choice is

$$\sigma_0=\sigma(\beta,\gamma_i,h_i)=\frac{e^{-\beta\mathcal{H}(\gamma_i,h_i,0)}}{\text{Tr}\left[e^{-\beta\mathcal{H}(\gamma_i,h_i,0)}\right]}. \quad (81)$$

We then time evolve with $\mathcal{H}(\gamma_f,h_f,U)$ and are interested in the following Green's functions

$$\mathcal{G}_{+-}(i,j;t)=\text{Tr}\left[c_i^\dagger(t)c_j(t)\sigma_0\right]\,,$$
$$\mathcal{G}_{++}(i,j;t)=\text{Tr}\left[c_i^\dagger(t)c_j^\dagger(t)\sigma_0\right]. \quad (82)$$

Details regarding the implementation of the EOM formalism are presented in Appendix D. Figure 30 shows results for the Green's functions (82) for a system prepared in the density matrix $\sigma(\infty,0.2,0)$ and time evolved with $\mathcal{H}(0.5,0.1,U)$. In the integrable case $U=0$ we observe relaxation towards the appropriate GGE. On the other hand, in the non-integrable case $U=0.1$ we observe a PT plateau. This analysis establishes that PT is robust under $U(1)$ symmetry breaking.

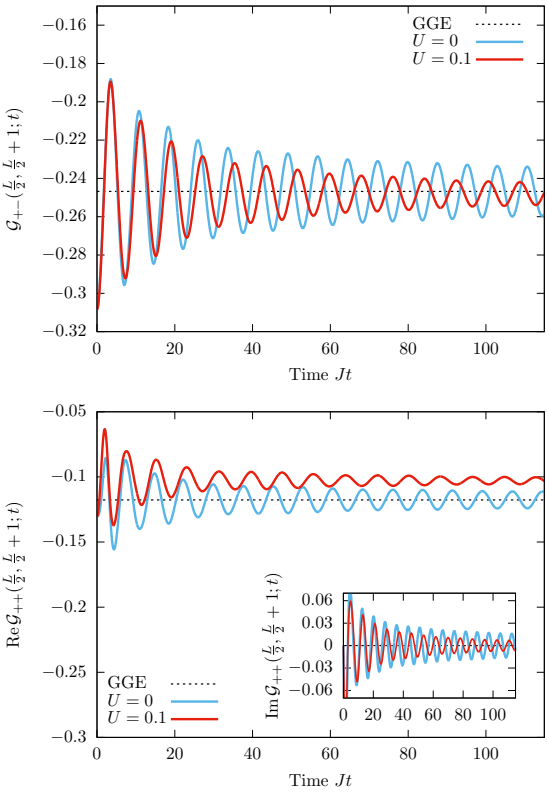

FIG. 30. $\mathcal{G}_{+-}(L/2,L/2+1;t)$ (top) and $\mathcal{G}_{++}(L/2,L/2+1;t)$ (bottom) for a system prepared in the state $\sigma(\infty,0.2,0)$ and time evolved with $\mathcal{H}(0.5,0.5,0.1)$. Dotted lines denote the non-interacting GGE.

A. Pre-relaxation

An interesting limit of the model (80) is the case when $h=O(U)$, *i.e.* the chemical potential is included in the integrability-breaking perturbation. Then the "unperturbed" integrable model is related to the XY chain in zero magnetic field by a Jordan-Wigner transformation. The XY chain is known to possess infinitely many local conservation laws $\{\mathcal{Q}_n\}$ that satisfy a non-abelian commutation algebra,[69] as well as a infinite set of mutually commuting local conserved charges $\{\mathcal{I}_n\}$.

Reference [71] investigated how the additional conservation laws influence the time evolution in the presence of an interacting perturbation which breaks this structure. The problem was studied using a novel mean-field-like technique which was conjectured to be accurate for times $t\sim U^{-1}$. It was found that observables show highly non-trivial behaviour if one starts from an initial state in which some of the additional charges have non-zero expectation values. In this situation, observables rapidly relax towards values close to the unperturbed GGE prediction (which describes the stationary state for $U=0$) and then, at times $t\sim U^{-1}$, drift away. Two scenarios are possible at this point: either the observables relax *towards a second nonthermal plateau* which is $\mathcal{O}(U^0)$ different from the first, or they *show persistent oscillations* within the entire accessible time-window. This phenomenon was termed *pre-relaxation* because it describes the crossover between two *non-thermal* behaviours. In the case where the introduced perturbation breaks integrability, the system is believed to eventually thermalize, although the thermalization time-scales are beyond the time regime that is accessible to the method of Ref. [71].

The Hamiltonian (80) for $h=\mathcal{O}(U)$ is precisely one of the cases considered in Ref. [71], once spins are mapped to fermions. Moreover, the time scale $t\sim U^{-1}$ on which the mean-field-like approach was conjectured to be accurate is amenable to analysis by our first-order EOM and it is interesting to compare the two results. To perform

the comparison, we consider the correlation function

$$\mathcal{S}(i;t) \equiv \mathrm{Re}\left[\mathcal{G}_{++}(i+1,i;t) - \mathcal{G}_{+-}(i+1,i;t)\right] , \quad (83)$$

which corresponds, through a Jordan-Wigner transformation, to $\langle \sigma_i^x \sigma_{i+1}^x \rangle (t)$ in the spin model. As the additional "non-abelian" local conservation laws $\mathcal{Q}_n$ of the XY chain change sign under translation by one site, we require an initial state that is not invariant under translations by one site. In order for the $\mathcal{Q}_n$ to have non-vanishing expectation values. To compare to the results of Ref. [71], we take the initial state to be the ground state of the Majumdar-Ghosh (MG) Hamiltonian,[131] which is invariant only under translations by two sites. Expectation values in the initial state can be calculated using Wick's theorem, as required for the EOM to be applicable, and the initial Green's functions read

$$\begin{aligned} \mathcal{G}_{+-}(2i-r,2j-s;0)\big|_{\mathrm{MG}} &= \delta_{i-r,j-s} , \quad r,s = 0,1 \\ \mathcal{G}_{++}(i,j;0)\big|_{\mathrm{MG}} &= 0 . \end{aligned} \quad (84)$$

In Fig. 31 we report a comparison between the mean-field approach of Ref. [71] and the first order EOM. The mean-field solution starts from the prediction of the non-interacting GGE and it is in excellent agreement with the EOM. The agreement is almost perfect because the interaction is very small in the case considered, but in general we do expect $\mathcal{O}(U)$ differences between the two results.

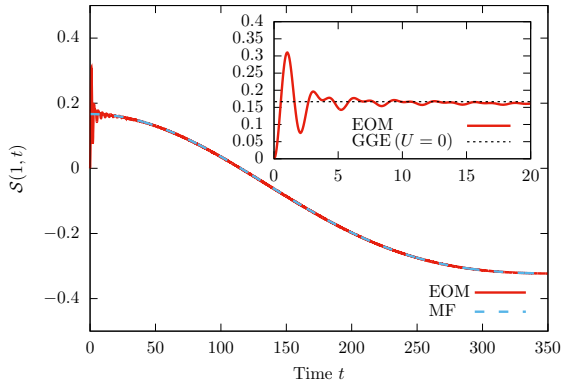

FIG. 31. $\mathcal{S}(1;t)$ (*cf.* Eq. (83)) evolved by $\mathcal{H}(2, 0.005, 0.005)$, starting from the ground state of the Majumdar-Ghosh Hamiltonian.[131] The full line is obtained by integration of the first order EOM (reported in Appendix D), while the dashed lines are the prediction of the mean-field approach developed in [71]. The inset shows a shorter time window where the observable lies on the first quasi-stationary plateau (black dotted line).

IX. CONCLUSIONS

In this work we have used equation of motion techniques to investigate prethermalization in a class of one dimensional fermion models with weak integrability breaking perturbations. Our integrable model is a non-interacting theory, and the role of the integrability breaking perturbation is played by density-density interactions. We focus on the time evolution of the single-particle Green's function after initializing the system in a density matrix that is not an eigenstate of the time evolution operator.

The non-equilibrium evolution in the non-interacting theory is non-trivial in our setup and provides an important point of reference. As expected expectation values of local operators relax towards GGEs in this case. When we turn on a weak integrability breaking perturbation of strength U, we observe long lived PT plateaux: the Green's function (for finite separations) relaxes towards constant values that differ from the ones in the GGE at order $\mathcal{O}(U)$, and are compatible with the deformed GGE description proposed in Ref. [67]. We have verified that PT occurs irrespective of whether particle number is conserved. This is in accord with expectations based on the CUT approach to non-equilibrium evolution[62,67]: as long as the integrability-breaking perturbation merely *dresses* the elementary excitations of the non-interacting theory we expect PT to occur. For very weak perturbations U the PT plateau is stable throughout the time window accessible to us. By increasing U we are able to observe a crossover between PT and evolution towards a thermal steady state. The corresponding crossover time scales as U^{-2}.

We have used our EOM methods to analyze the structure of light-cones in the single-particle Green's function. Light cone effects provide a direct probe of quasi-particle properties, and it is clearly an interesting question how these are affected by integrability breaking terms. We observed that in all cases the exterior and interior regions of the light-cone are separated by an "intermediate" regime, the width of which appears to scale with a universal exponent $t^{1/3}$ irrespective of whether or not the post-quench Hamiltonian is integrable. In contrast, the maximum values of the real and imaginary parts of the single-particle Green's function, *i.e.* our "signals", exhibit a markedly faster decay in time t in the non-integrable case as compared to the integrable one.

Our work raises a number of issues deserving of further investigation. First, our work suggests that PT is rather robust provided the integrability breaking perturbation does not dramatically alter the nature of quasi-particle excitations. It would be interesting to analyze examples where we know confinement to occur, an example being the transverse field Ising model in a weak longitudinal magnetic field.[123,132,133] Unfortunately such situations cannot be accommodated in the EOM approach, because the perturbation is non-local in terms of the elementary fermions. Second, our approach is by construction uncontrolled. We have checked that our results are in excellent agreement with existing t-DMRG results,[67] but further checks are highly desirable. We also expect our truncation of the infinite hierarchy of EOMs to be-

come inaccurate at late times. It would be interesting to try to implement a truncation scheme that incorporates effects of the four particle cumulant. This is numerically very demanding, but would open the possibility of exploring the late time regime.[96]

Finally, it would be very interesting to investigate the analogous set of questions for a weak perturbation to a strongly interacting integrable model.

ACKNOWLEDGMENTS

We thank John Cardy, Maurizio Fagotti, Stefan Kehrein, Robert Konik and Wei Ku for useful discussions surrounding this work. FE and NR thank Salvatore Manmana for the previous collaboration [67] on this problem. This work was supported by the EPSRC under grants EP/I032487/1 (BB and FHLE) and EP/J014885/1 (FHLE), the Isaac Newton Institute for Mathematical Sciences under grant EP/K032208/1, the ERC under Starting Grant 279391 EDEQS (BB), the U.S. Department of Energy under Contract No. DE-SC0012704 (NJR), and by the Clarendon Scholarship fund (SG).

Appendix A: Further details on the time evolution of the Green's function

In this appendix we collect some results on how the time evolution of $\mathcal{G}(j,l;t)$ is influenced by (i) particle-hole symmetry, (ii) final dimerization, (iii) sign of the interaction.

1. The role of particle-hole symmetry

For a given interaction strength U, we have seen that the addition of next-neighbour hopping ($J_2 > 0$) to the Hamiltonian has a significant effect on the time evolution of local observables – they show a marked drift towards their thermal values. To investigate whether this effect is related to the breaking of particle-hole symmetry by the J_2 term, we study the time evolution with a modified Hamiltonian where we replace the next-neighbour hopping with a next-next-neighbour term, J_3. Such a modification preserves particle-hole symmetry, whilst modifying the single-particle dispersion to introduce more crossings at a fixed energy. Specifically, we consider

$$H_3(J_3,\delta,U) = H(0,\delta,U) - J_3 \sum_{i=1}^{L} \left(c_i^\dagger c_{i+3} + \text{h.c.} \right) . \quad \text{(A1)}$$

The EOM analysis proceeds as before, provided one uses the appropriately modified single-particle dispersion and

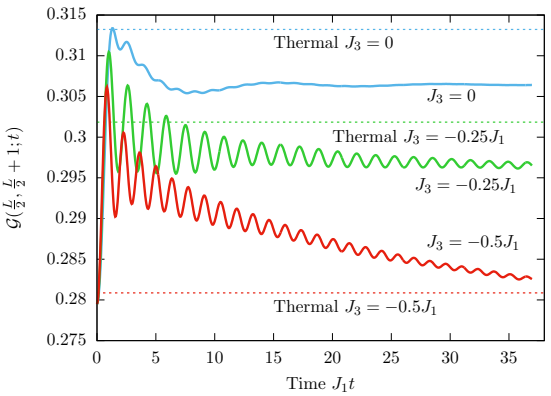

FIG. 32. Green's function $\mathcal{G}(L/2, L/2+1; t)$ for a systems of sizes $L = 320, 384$ that is prepared in the density matrix $\rho_0(2,0)$ and time-evolved with $H_3(J_3, 0.1, 0.4)$ [*cf.* (A1)]. The expected steady state thermal values computed by ED for $L = 16$ are shown by dotted lines. We note that the cases with $J_3 \neq 0$ exhibit pronounced finite-size effects in the ED data.

Bogoliubov angle

$$\epsilon_\eta(k,\delta_f,J_3) = 2\eta\sqrt{(\cos(k) + J_3\cos(3k))^2 + \delta_f^2 \sin^2(k)} \ ,$$
$$e^{-i\varphi_k(\delta_f,J_3)} = \frac{-(\cos k + J_3\cos(3k)) + i\delta_f \sin k}{\sqrt{(\cos(k) + J_3\cos(3k))^2 + \delta_f^2 \sin^2 k}} \ . \quad \text{(A2)}$$

In Fig. 32, we show that *drifting towards the thermal values also occurs when particle-hole symmetry is preserved.* Instead, it appears that the presence of multiple crossings at fixed energy ("scattering channels") in the single particle dispersion (*cf.* Fig. 33) is the key ingredient for observing the drift towards thermalization in achievable time scales. As for the case with J_2, the higher the degeneracy at fixed energy in the single particle dispersion, the stronger the drifting becomes. We stress that there is no enhancement of the effective interaction with increasing $|J_3|$ (*cf.* Sec. V A), as the bandwidths of both bands are (slightly) *increased* by the addition of $|J_3|$.

As an aside, we note that the initial relaxation towards the PT plateau is much slower in the $J_3 \neq 0$ case. For large positive J_3, relaxation takes places at times much larger than those reachable with the EOM. The slow decay of oscillation towards PT can be understood from the leading order EOM (38), see also Ref. [67]. Inserting the solution of Eq. (38) into Eq. (21), one obtains the prethermal behaviour of the Green's function. By means of a stationary phase analysis, it can be seen that the relaxation of the Green's function towards the PT plateau is generically $t^{-1/2}$ for $J_3 \neq 0$, compared to $t^{-3/2}$ when $J_3 = 0$. For the cases reported in Fig. 32, the leading $t^{-1/2}$ term has a small pre-factor, and one effectively sees oscillations whose amplitude decays as $1/t$.

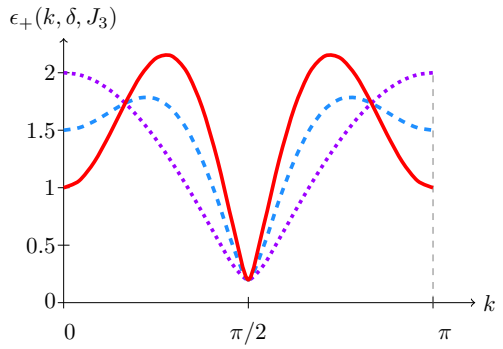

FIG. 33. Dispersion relation $\epsilon_+(k,\delta,J_3) = -\epsilon_-(k,\delta,J_3)$ [see Eq. (A2)] for the two bands of Bogoliubov fermions in the non-interacting model with $J_1 = 1$, $\delta = 0.1$ and $J_3 = 0$ (dotted), $J_3 = -0.25$ (dashed), $J_3 = -0.5$ (solid). Increasing J_3 leads to additional crossings at a fixed energy.

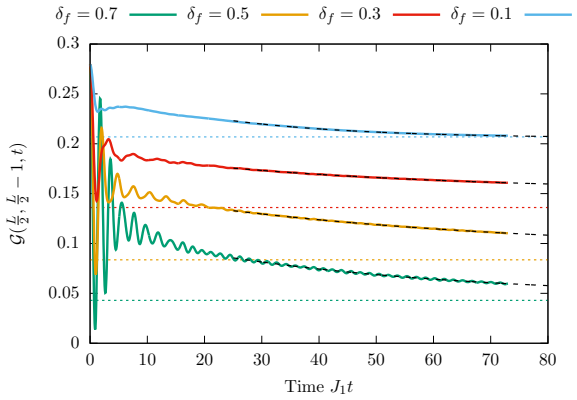

FIG. 34. The Green's function $\mathcal{G}(L/2, L/2-1; t)$ for a system of size $L = 320$ that is prepared in the density matrix $\rho_0(2,0)$ and time-evolved with $H(0.5,\delta_f,0.4)$ [*cf.* (1)] with $\delta_f = 0.1, 0.3, 0.5, 0.7$ (top to bottom). The expected steady state thermal values are shown by dotted lines.

2. Dependence on dimerization parameter δ_f

We now turn to the dependence of the post-quench dynamics on the nearest-neighbour dimerization δ_f, which without loss of generality can be taken in the range $0 \le \delta_f \le 1$. In Fig. 34 we show the time-evolution of the Green's function when the system is initialized in the density matrix $\rho_0(2,0)$ and time evolved with $H(0.5,\delta_f,0.4)$ for a range of values of δ_f. As we increase δ_f we initially observe a decrease in the inverse relaxation times.

a. Restoration of translational symmetry: $\delta_f = 0$

In the special case $\delta_f = 0$ our post-quench Hamiltonian is translationally invariant by one site (rather than two). This allows us to address the issue of translational symmetry restoration: if we start in an initial state that is invariant only under translations by two sites, is one-site translational symmetry restored at long times after the quench? To address this question, we consider the time-evolution of the initial density matrix (14) with $\beta_i = 2$, $\delta_i = 0.5$ with the Hamiltonian (1) with $J_2 = 0.5$, $\delta_f = 0$ and $U = 0.4$. Figure 35 show results for the Green's function with separation ± 1. In both cases we see that there is a rapid restoration of translational symmetry – by time $J_1 t \sim 10$ the results are already extremely close. The situation for larger separations is completely analogous, but the time scale after which symmetry restoration is seen is pushed back, as expected.

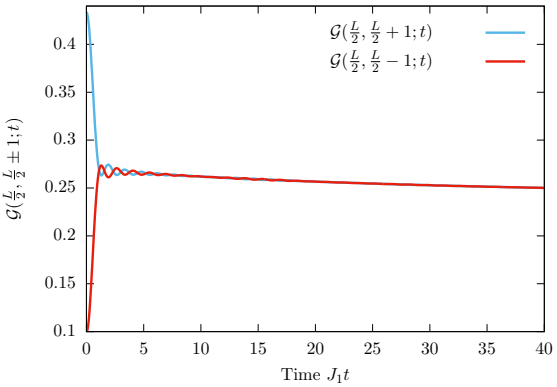

FIG. 35. Time evolution of $\mathcal{G}(L/2, L/2\pm 1; t)$ for a system initialized in the density matrix $\rho_0(2,0,5)$ (14) and time evolved with the translationally invariant Hamiltonian $H(0.5,0,0.4)$.

3. Attractive interactions

In the main text we have focused on repulsive interactions $U > 0$ in the Hamiltonian (1). Here we briefly consider the case of attractive interactions. In Fig. 36 we compare the results for the time evolution of the Green's function at separation 1 for interactions strengths $U = \pm 0.4$. We see that the results look broadly similar. The most marked difference is observed for intermediate times ($5 \lesssim t \lesssim 30$ in the figure). The same holds true for larger separations. This is accordance with our expectation: in the intermediate (PT) time-window the Green's functions in the two cases are generically order U different, but at late enough times their evolution is described by the same quantum Boltzmann equation.

Appendix B: Perturbative calculation of the thermal values

In this appendix we compute the thermal expectation values

$$n_{\mu\nu}(k) \equiv \langle \alpha^\dagger_\mu(k)\alpha_\nu(k)\rangle \tag{B1}$$

$$\equiv \frac{1}{Z}\mathrm{Tr}\left[\alpha^\dagger_\mu(k)\alpha_\nu(k)e^{-\beta_{\rm eff}(H-\mu N)}\right], \tag{B2}$$

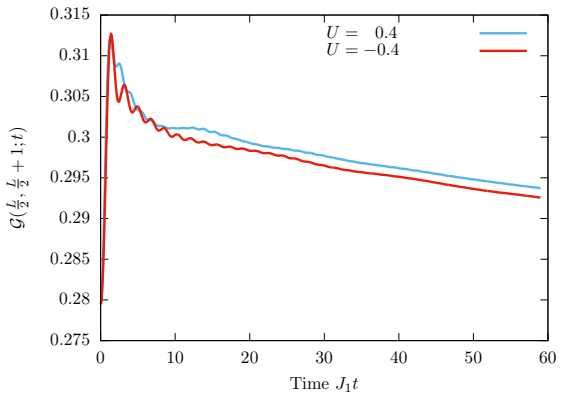

FIG. 36. The Green's function $\mathcal{G}(L/2, L/2+1; t)$ with time-evolution generated by (blue) $H(0.5, 0.1, 0.4)$ and (red) $H(0.5, 0.1, -0.4)$. The system starts from the thermal state (14) with $\beta_i = 2$, $J_2 = 0$, $\delta_i = 0$ and $U = 0$.

where $Z \equiv \mathrm{Tr}\left[e^{-\beta_{\mathrm{eff}}(H-\mu N)}\right]$ and we use the shorthand notation $H \equiv H(J_2, \delta_f, U)$. The inverse temperature β_{eff} and the chemical potential μ_{eff} are fixed by requiring

$$\langle H \rangle_0 = \frac{1}{Z}\mathrm{Tr}\left[He^{-\beta_{\mathrm{eff}}(H-\mu_{\mathrm{eff}}N)}\right] , \tag{B3}$$

$$\langle N \rangle_0 = \frac{1}{Z}\mathrm{Tr}\left[Ne^{-\beta_{\mathrm{eff}}(H-\mu_{\mathrm{eff}}N)}\right] , \tag{B4}$$

where $\langle\cdot\rangle_0$ is the expectation value in the initial state. In order to compute the finite-temperature mode occupation numbers (B2), we compute the thermal propagator

$$G_{\mu\nu}(\tau, k) = \langle T_\tau \left[\alpha^\dagger_\mu(\tau, k)\alpha_\nu(0, k)\right]\rangle , \tag{B5}$$

$$\alpha^\dagger_\mu(s, k) \equiv e^{sH}\alpha^\dagger_\mu(k)e^{-sH} , \tag{B6}$$

using finite-temperature perturbation theory to the order U^2. The thermal mode occupation numbers can be recovered from the thermal propagator using

$$n_{\mu\nu}(k) = \lim_{\tau\to 0^+} G_{\mu\nu}(\tau, k) = \frac{1}{\beta_{\mathrm{eff}}}\sum_{\omega_n} G_{\mu\nu}(\omega_n, k)e^{i\omega 0^+} . \tag{B7}$$

Writing the Green's function in matrix notation, the single particle self energy $\mathbf{\Sigma}(\omega_n, k)$ is defined by the Dyson equation

$$\mathbf{G}(\omega_n, k)^{-1} = \mathbf{G_0}(\omega_n, k)^{-1} - \mathbf{\Sigma}(\omega_n, k) \tag{B8}$$

where

$$(G_0)_{\mu\nu}(\omega_n, k) = \frac{\delta_{\mu\nu}}{i\omega_n - \bar{\epsilon}_\mu(k)} \tag{B9}$$

and $\bar{\epsilon}_\eta(k) \equiv \epsilon_\eta(k) - \mu_{\mathrm{eff}}$. The Feynman rules read:

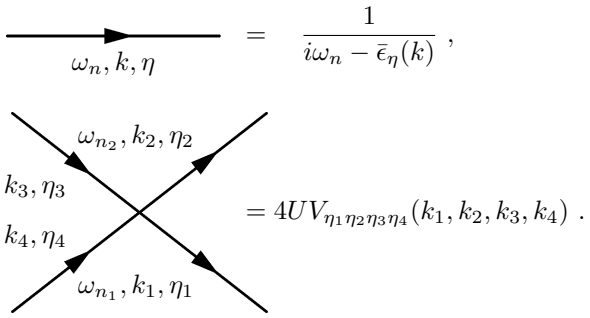

with conservation of ω at each vertex. Therefore the diagrams contributing to the self energy to second order are

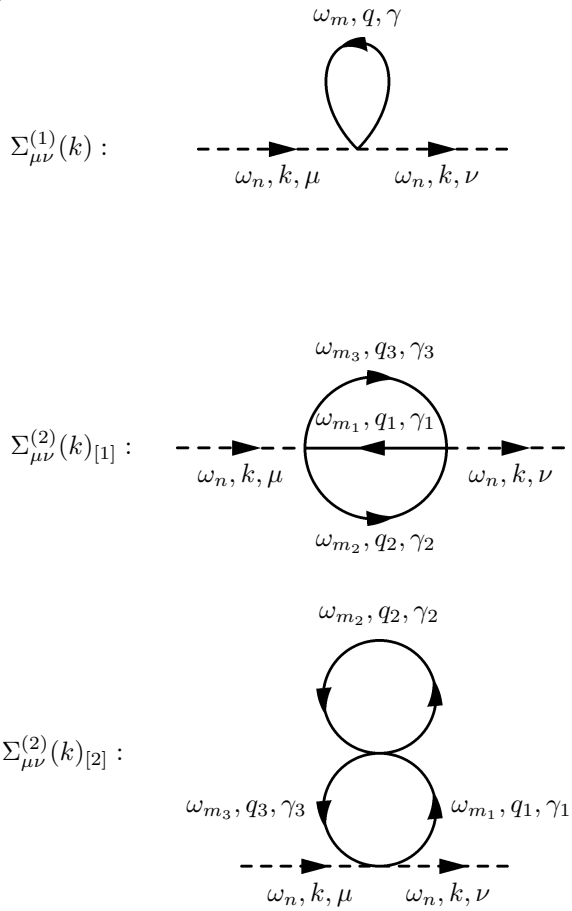

where the incoming and outgoing legs are amputated. Evaluating these, we find:

$$\Sigma^{(1)}_{\mu\nu}(k) \equiv 4U \sum_{q,\gamma} V_{\nu\gamma\gamma\mu}(k,q,q,k) n(\bar{\epsilon}_\gamma(q)) \ , \tag{B10}$$

$$\Sigma^{(2)}_{\mu\nu}(k)_{[1]} \equiv -4U \sum_{\gamma_1,\gamma_3,q_1} \Sigma^{(1)}_{\gamma_1\gamma_3}(q_1) V_{\nu\gamma_1\gamma_3\mu}(k,q_1,q_1,k) n(\bar{\epsilon}_{\gamma_1}(q_1)) \tilde{n}(\bar{\epsilon}_{\gamma_3}(q_1)) f(\epsilon_{\gamma_1\gamma_3}(q_1)) \ , \tag{B11}$$

$$\begin{aligned}\Sigma^{(2)}_{\mu\nu}(\omega,k)_{[2]} \equiv 8U^2 \sum_{\{\gamma_i\}} \sum_{\{q_i\}} \Big\{ & V_{\nu\gamma_1\gamma_2\gamma_3}(k,q_1,q_2,q_3) V_{\gamma_3\gamma_2\gamma_1\mu}(q_3,q_2,q_1,k) n(\bar{\epsilon}_{\gamma_1}(q_1)) \\ & \times \tilde{n}(\bar{\epsilon}_{\gamma_2}(q_2)) \tilde{n}(\bar{\epsilon}_{\gamma_3}(q_3)) f(i\omega + \bar{\epsilon}_{\gamma_1}(q_1) - \bar{\epsilon}_{\gamma_2}(q_2) - \bar{\epsilon}_{\gamma_3}(q_3)) \Big\} \ .\end{aligned} \tag{B12}$$

with the functions $\tilde{n}(x) \equiv 1 - n(x)$, $n(x)$ being the Fermi-Dirac distribution and $f(x) \equiv \frac{e^{\beta_{\text{eff}} x} - 1}{x}$. Using the Dyson equation for the propagator (B8), expanding to second order in the self energy and inserting into Eq. (B7), we find the thermal mode occupation numbers up to $O(U^2)$

$$\begin{aligned} n_{\mu\nu}(k,\beta_{\text{eff}},\mu) = & \delta_{\mu,\nu}\ n(\bar{\epsilon}_\mu(k)) - (\Sigma^{(1)}_{\mu\nu}(k) + \Sigma^{(2)}_{\mu\nu}(k)_{[1]}) n(\bar{\epsilon}_\mu(k)) \tilde{n}(\bar{\epsilon}_\nu(k)) f(\epsilon_{\mu\nu}(k)) \\ & + \sum_\delta \frac{\Sigma^{(1)}_{\mu\delta}(k)\Sigma^{(1)}_{\delta\nu}(k)}{\epsilon_{\mu\delta}(k)\epsilon_{\delta\nu}(k)\epsilon_{\mu\nu}(k)} \Big(n(\bar{\epsilon}_\mu(k))\epsilon_{\delta\nu}(k) - n(\bar{\epsilon}_\delta(k))\epsilon_{\mu\nu}(k) + n(\bar{\epsilon}_\nu(k))\epsilon_{\mu\delta}(k) \Big) \\ & + 8U^2 \sum_{\{\gamma_i\}} \sum_{\{q_i\}} \Big\{ V_{\mu\gamma_1\gamma_2\gamma_3}(k,q_1,q_2,q_3) V_{\gamma_3\gamma_2\gamma_1\nu}(q_3,q_2,q_1,k) \tilde{n}(\bar{\epsilon}_{\gamma_3}(q_3)) \tilde{n}(\bar{\epsilon}_{\gamma_2}(q_2)) \\ & \times n(\bar{\epsilon}_{\gamma_1}(q_1)) G_{\mu\nu\gamma_1\gamma_2\gamma_3}(k,q_1,q_2,q_3) \Big\} \ . \end{aligned} \tag{B13}$$

where we set

$$G_{\mu\nu\gamma_1\gamma_2\gamma_3}(k,q_1,q_2,q_3) = \frac{1}{\epsilon_{\mu\nu}(k)} \sum_{\eta=\pm} \{ (\delta_{\eta,\mu} - \delta_{\eta,\nu}) n(\bar{\epsilon}_\eta(k)) f(E_{\eta\gamma_1\gamma_2\gamma_3}(k,q_1,q_2,q_3)) \} \ . \tag{B14}$$

Appendix C: Boltzmann Equation for $\delta_f \neq 0$

The numerical solution of the EOM (34) for $\delta_f \neq 0$ suggests that at sufficiently late times the occupation numbers assume the form

$$n_{\mu\mu}(k,t) = s_\mu(k, U^2 t) + \Delta_\mu(k,t) \ , \tag{C1}$$

where $s_\mu(k,U^2t)$ is a smooth, slowly varying function of time and $\Delta_\mu(k,t)$ is a small highly oscillatory contribution. As we are interested in the single particle Green's function in position space, the contributions arising from $\Delta_\mu(k,t)$ will be negligible at late times. As we will now argue, the smooth component $s_\mu(k,U^2t)$ fulfils a QBE in the Boltzmann limit (63).

Our starting point are the EOM for the occupation numbers, where we neglect all contributions involving the off-diagonal two-point functions $\{n_{+-}(k,t)\}$ as at late times they are $\mathcal{O}(U)$ and rapidly oscillating. The "reduced" EOMs can be written in the following compact form

$$\dot{n}_{\mu\mu}(k,t) = U D_\mu(k,t) + U^2 I_\mu[\{n_{\nu\nu}\}](k,t) \ , \tag{C2}$$

where we introduced

$$D_\mu(k,t) = 8\text{Im}\Big[(A_{\bar{\mu}}(k) + B_{\bar{\mu}}(k,t))\, n_{\mu\bar{\mu}}(k) e^{i\epsilon_{\mu\bar{\mu}}(k)t} \Big] \ . \tag{C3}$$

Here $A_{\bar{\mu}}(k)$ and $B_{\bar{\mu}}(k,t)$ are defined in Eqs. (60) and (61) respectively and

$$\begin{aligned} I_\mu[\{n_{\nu\nu}\}](k,t) \equiv & -\int_0^t \mathrm{d}s \sum_{\boldsymbol{\gamma}} \sum_{k_1,k_2>0} K^{\boldsymbol{\gamma}}_{\mu\mu}(k_1,k_2;k;t-s) n_{\gamma_1\gamma_2}(k_1,s) n_{\gamma_3\gamma_4}(k_2,s) \delta_{\gamma_1,\gamma_2}\delta_{\gamma_3,\gamma_4} \\ & - \int_0^t \mathrm{d}s \sum_{\vec{\gamma}} \sum_{k_1,k_2,k_3>0} L^{\vec{\gamma}}_{\mu\mu}(k_1,k_2,k_3;k;t-s) n_{\gamma_1\gamma_2}(k_1,s) n_{\gamma_3\gamma_4}(k_2,s) n_{\gamma_5\gamma_6}(k_3,s) \delta_{\gamma_1,\gamma_2}\delta_{\gamma_3,\gamma_4}\delta_{\gamma_5,\gamma_6} \ , \end{aligned} \tag{C4}$$

where the kernels are defined in Eq. (35). Substituting (C1) into (C2) we obtain

$$U^2\partial_\tau s_\mu(k,\tau)\big|_{\tau=U^2t} + \partial_t\Delta_\mu(k,t) = UD_\mu(k,t) + U^2 I_\mu[\{s_\nu+\Delta_\nu\}](k,t)\,. \tag{C5}$$

We now remove the rapidly oscillating part of (C5) by acting with a low-pass filter and then take the Boltzmann scaling limit (63). We employ a filter of the form

$$\begin{aligned}\mathcal{L}[f(t)] &\equiv \int_{-\infty}^{\infty} \mathrm{d}s\ \ell(t-s,\omega_{\rm CUT})\ f(s)\ ,\\ \ell(t,\omega) &\equiv \int_{-\omega}^{\omega}\frac{\mathrm{d}\sigma}{2\pi}\ e^{i\sigma t} = \frac{\sin(\omega t)}{\pi t}\,.\end{aligned} \tag{C6}$$

The cutoff frequency $\omega_{\rm CUT}$ is chosen such that

$$\begin{aligned}\mathcal{L}[\partial_t^n s_\mu(k,U^2t)] &= \partial_t^n s_\mu(k,U^2t)\,,\quad n=0,1,\dots\ ,\\ \mathcal{L}\left[e^{i\omega t}\right] &= 0\,,\qquad \text{for}\qquad \omega=\mathcal{O}(1)\,.\end{aligned} \tag{C7}$$

These two requirements can be met by choosing $\omega_{\rm CUT}\sim U^\alpha$ with $0<\alpha<2$. Applying the filter to the EOM (C2) and taking the Boltzmann scaling limit (63) we find

$$\partial_\tau s_\mu(k,\tau) = \lim_{sc}\mathcal{L}\left[I_\mu[\{s_\nu+\Delta_\nu\}](k,t)\right]\,. \tag{C8}$$

Here we have used that $|\epsilon_{\mu\bar\mu}(k)|$ is bounded from below by a constant of order one, which implies that $D_\mu(k,t)$ is rapidly oscillating at late times. Let us now study the effect of the low-pass filter combined with the Boltzmann scaling limit on the functional I_μ. Because of the linearity of the filter we have

$$\begin{aligned}\mathcal{L}[I_\mu[\{s_\nu+\Delta_\nu\}](k,t)] &= \mathcal{L}\left[I_\mu[\{s_\nu\}](k,t)\right]\\ &+\mathcal{L}\left[I_\mu[\{s_\nu+\Delta_\nu\}](k,t) - I_\mu[\{s_\nu\}](k,t)\right]\,.\end{aligned} \tag{C9}$$

The term $I_\mu[\{s_\nu\}](k,t)$ is of the same form as the one considered in Eq. (67). It can be cast in the form

$$I_\mu[\{s_\nu\}](k,t) = \sum_{\boldsymbol{q}>0,\boldsymbol{\lambda}}\int_0^t \mathrm{d}s\ f^\mu_{\boldsymbol{\lambda}}(\mathbf{q},k;U^2s)e^{\mathrm{i}E_{\boldsymbol{\lambda}}(\mathbf{q})(t-s)}. \tag{C10}$$

Importantly $f^\mu_{\boldsymbol{\lambda}}(\mathbf{q},k;U^2s)$ depends on the variable s only through the combination U^2s. In writing (C10) we have assumed that in the scaling limit we can neglect the analogue of the first term in the right hand side of Eq. (67), and we have replaced the integration boundary $t-\bar t$ by t in the remaining contribution (which is justified by referring to the scaling limit). In order to ease notations we now focus on a single term to the sums in (C10) and suppress all unnecessary indices. It is convenient to define a function

$$\mathfrak{F}(s_1,E) = \int_0^{s_1}\mathrm{d}s_2\, f(U^2(s_1-s_2))e^{\mathrm{i}Es_2}. \tag{C11}$$

We now define the action of the low-pass filter by

$$\begin{aligned}\mathcal{L}[\mathfrak{F}(t,E)] &= \int_{-\infty}^0 \mathrm{d}s_1\frac{\sin(\omega_{\rm CUT}(t-s_1))}{\pi(t-s_1)}\mathfrak{F}(s_1,E-i\eta)\\ &+\int_0^\infty \mathrm{d}s_1\frac{\sin(\omega_{\rm CUT}(t-s_1))}{\pi(t-s_1)}\mathfrak{F}(s_1,E+i\eta)\\ &\equiv \Sigma_1+\Sigma_2.\end{aligned} \tag{C12}$$

where we have appropriately regularised the two integrals using an infinitesimal parameter η (*cf.* VII B). Importantly, we will exchange limits and keep η fixed when taking the Boltzmann scaling limit. Using that the derivatives of f are suppressed by powers of U^2, in the scaling limit we have

$$\begin{aligned}\Sigma_1 &\to \frac{i}{(E-i\eta)}\lim_{sc}\int_t^\infty \mathrm{d}s_1\frac{\sin(\omega_{\rm CUT}s_1)}{\pi s_1}f(U^2(t-s_1))\\ &= \frac{if(\tau)}{E-i\eta}\lim_{sc}\int_{-\infty}^\infty \mathrm{d}s_1\frac{\sin(\omega_{\rm CUT}s_1)}{\pi s_1}\,\theta_{\rm H}(s_1-t)\\ &= 0\,.\end{aligned} \tag{C13}$$

Here $\tau=U^2t$ and in the second step we have used that $\sin(\omega_{\rm CUT}s_1)/s_1$ is oscillating and peaked around $s_1=0$ with a width that scales as $\omega_{\rm CUT}^{-1}$, while $f(U^2(t-s_1))$ is essentially constant in that window. Going through the analogous steps for the second term in (C12) gives

$$\Sigma_2 \to \frac{if(\tau)}{E+i\eta}\int_{-\infty}^\infty \mathrm{d}s_1\frac{\sin(s_1)}{\pi s_1} = D(E)f(\tau)\,, \tag{C14}$$

where $D(E)$ is defined in Eq. (69). Putting everything together we conclude that

$$\lim_{sc}\mathcal{L}\left[I_\mu[\{s_\mu\}](k,t)\right] = \tilde I_\mu[\{s_\mu\}](k,\tau)\,, \tag{C15}$$

where

$$\tilde I_\mu[\{s_\mu\}](k,\tau) \equiv -\sum_{\gamma,\eta}\sum_{p,q>0}\widetilde K_\mu^{\gamma\eta}(p,q|k)s_\gamma(p,\tau)s_\eta(q,\tau) - \sum_{\gamma,\eta,\epsilon}\sum_{p,q,r>0}\widetilde L_\mu^{\gamma\eta\epsilon}(p,q,r|k)s_\gamma(p,\tau)s_\eta(q,\tau)s_\epsilon(r,\tau)\,. \tag{C16}$$

The various kernels appearing in (C16) are defined in Eq. (71).

We now turn to the second term in (C9). This is more difficult to treat, because of the oscillating con-

tributions to the occupation numbers. The difference $I_\mu[\{s_\nu+\Delta_\nu\}](k,t)-I_\mu[\{s_\nu\}](k,t)$ can be cast in the form

$$\sum_{\boldsymbol{q}>0,\boldsymbol{\lambda}}\sum_i\int_0^t \mathrm{d}s\; h^{\mu,\,i}_{\boldsymbol{\lambda}}(\mathbf{q},k;U^2s)e^{i\varepsilon_{\boldsymbol{\lambda},\,i}(\mathbf{q})s}e^{\mathrm{i}E_{\boldsymbol{\lambda}}(\mathbf{q})(t-s)}. \tag{C17}$$

In order to proceed we now make the assumption that, as a function of $\mathbf{q}$, $\varepsilon_{\boldsymbol{\mu},\,i}(\mathbf{q})$ is generically of order one and vanishes only on a set of measure zero. When applying the low-pass filter to (C17) it useful to distinguish between two cases: (i) $\varepsilon_{\boldsymbol{\mu},\,i}(\mathbf{q})\neq E_{\boldsymbol{\mu}}(\mathbf{q})$ except on a set of measure zero; (ii) $\varepsilon_{\boldsymbol{\mu},\,i}(\mathbf{q})=E_{\boldsymbol{\mu}}(\mathbf{q})$. We now again ease notations by focussing on a single term and suppressing all indices. It is convenient to define a function

$$\mathfrak{H}(s_1,E)=e^{\mathrm{i}\varepsilon s_1}\int_0^{s_1}\mathrm{d}s_2\,h(U^2(s_1-s_2))e^{\mathrm{i}Es_2}. \tag{C18}$$

Proceeding as before, we define the action of the low-pass filter by

$$\begin{aligned}\mathcal{L}[\mathfrak{H}(t,E)] &= \int_{-\infty}^0 \mathrm{d}s_1\frac{\sin(\omega_{\mathrm{CUT}}(t-s_1))}{\pi(t-s_1)}\mathcal{H}(s_1,E-i\eta)\\ &\quad+\int_0^\infty \mathrm{d}s_1\frac{\sin(\omega_{\mathrm{CUT}}(t-s_1))}{\pi(t-s_1)}\mathfrak{H}(s_1,E+i\eta)\\ &\equiv \Sigma_3+\Sigma_4.\end{aligned} \tag{C19}$$

Considering the first term, we have in the scaling limit

$$\begin{aligned}\Sigma_3 &\to \lim_{sc}\int_{-\infty}^0 \mathrm{d}s_1\frac{\sin(\omega_{\mathrm{CUT}}(t-s_1))}{\pi(t-s_1)}\frac{ih(U^2s_1)e^{i\varepsilon s_1}}{(E-\varepsilon-i\eta)}\\ &= 0.\end{aligned} \tag{C20}$$

Here we used that $t\omega_{\mathrm{CUT}}$ tends to infinity in the scaling limit. Similarly we obtain

$$\begin{aligned}\Sigma_4 &\to \frac{ih(\tau)}{E-\varepsilon+i\eta}\lim_{sc}\int_{-\infty}^t \mathrm{d}s_1 e^{i\varepsilon t}\frac{\sin(\omega_{\mathrm{CUT}}s_1)}{\pi s_1}e^{-i\varepsilon s_1}\\ &= 0\,.\end{aligned} \tag{C21}$$

Finally, let us consider case (ii) defined above. Focussing again on a single contribution we now have

$$\int_{-\infty}^\infty \mathrm{d}s_1\, e^{iEs_1}\frac{\sin(\omega_{\mathrm{CUT}}(t-s_1))}{\pi(t-s_1)}\int_0^{s_1}\mathrm{d}s_2\,h(U^2s_2)\,. \tag{C22}$$

The function $\int_0^t \mathrm{d}s\,h(U^2s)$ does not contain highly oscillatory contributions and thus it can not counter balance the rapidly oscillating phase e^{iEt}. As a consequence the contribution (C22) vanishes in the scaling limit. This conclusion holds true even if an appropriate regularization of $\int_0^t \mathrm{d}s\,h(U^2s)$ is considered in order to deal with the limits $t\to\pm\infty$ (similarly to the cases considered before).

Putting everything together we conclude that the in the scaling limit the smooth parts $s_\mu(k,\tau)$ of the mode occupation numbers fulfil

$$\dot{s}_\mu(k,\tau)-\tilde{I}_\mu[\{s_\nu\}](k,\tau)=0\,, \tag{C23}$$

which has precisely the same form as the Quantum Boltzmann equation (70).

Appendix D: First order EOM for the U(1)-breaking case

Here we present some details regarding the first order EOM analysis of Sec. VIII. The first step is to move to momentum space. We do this by working with a 2-site elementary cell which allows us to accommodate e.g. initial states that are invariant only under translations by two sites. We define canonical momentum space fermion operators by

$$\begin{aligned}e_{k_n} &= \sqrt{\frac{2}{L}}\sum_j e^{ik_n(2j)}c_{2j}\;,\\ f_{k_n} &= \sqrt{\frac{2}{L}}\sum_j e^{ik_n(2j-1)}c_{2j-1}\;,\end{aligned} \tag{D1}$$

where $k_n=2\pi n/L$ with $n=1,\dots,L/2$. The Hamiltonian (80) is expressed as

$$\begin{aligned}\mathcal{H}(\gamma,h,U) &= J\sum_{k>0}\Big[\cos(k)f_k^\dagger e_k+i\gamma\sin(k)f_k^\dagger e^\dagger_{\pi-k}+\mathrm{h.c.}\Big]\\ &\quad-Jh\sum_{k>0}\Big[f_k^\dagger f_k+e_k^\dagger e_k\Big]\\ &\quad+4U\sum_{\boldsymbol{k}>0}W(\boldsymbol{k})e^\dagger_{k_1}e_{k_2}f^\dagger_{k_3}f_{k_4}\;,\end{aligned} \tag{D2}$$

where

$$\begin{aligned}W(\boldsymbol{k}) = \frac{1}{L}\big(&\delta_{k_1-k_2+k_3-k_4\pm\pi,0}\\ &+\delta_{k_1-k_2+k_3-k_4\pm\pi,0}\big)\cos(k_3-k_4)\;.\end{aligned} \tag{D3}$$

The EOMs are formulated for the fermion two point functions

$$\begin{aligned}v_1(k;t) &\equiv \mathrm{Tr}\left[f_k^\dagger(t)f_k(t)\sigma_0\right],\\ v_2(k;t) &\equiv \mathrm{Tr}\left[e_k^\dagger(t)e_k(t)\sigma_0\right],\\ v_3(k;t) &\equiv \mathrm{Tr}\left[f_k^\dagger(t)f^\dagger_{\pi-k}(t)\sigma_0\right],\\ v_4(k;t) &\equiv \mathrm{Tr}\left[e_k^\dagger(t)e^\dagger_{\pi-k}(t)\sigma_0\right],\\ v_5(k;t) &\equiv \mathrm{Tr}\left[f_k^\dagger(t)e_k(t)\sigma_0\right],\\ v_6(k;t) &\equiv \mathrm{Tr}\left[f_k^\dagger(t)e^\dagger_{\pi-k}(t)\sigma_0\right].\end{aligned} \tag{D4}$$

As with Sec. IV, we derive the first order EOM by writing the Heisenberg equations for the bilinears and neglecting the four-particle connected cumulants at all times. Defin-

ing $\bar{k} = \pi - k$ the result can be written in the form

$$\begin{aligned}
\dot{v}_1(k;t) &= 2\cos(k)\mathrm{Im}[v_5(k;t)] + 2\gamma\sin(k)\mathrm{Re}[v_6(k;t)] \\
&- 4Ui\sum_{q>0} W(q,k,k,q)v_5(q;t)v_5^*(k;t) \\
&+ 4Ui\sum_{q>0} W(k,q,q,k)v_5(k;t)v_5^*(q;t) \\
&+ 4Ui\sum_{q>0} W(q,\bar{q},k,\bar{k})v_6(q;t)v_6^*(k;t) \\
&- 4Ui\sum_{q>0} W(k,\bar{k},q,\bar{q})v_6(k;t)v_6^*(q;t), \qquad \text{(D5)}
\end{aligned}$$

$$\begin{aligned}
\dot{v}_2(k;t) &= -2\cos(k)\mathrm{Im}[v_5(k;t)] + 2\gamma\sin(k)\mathrm{Re}[v_6(\bar{k};t)] \\
&- 4Ui\sum_{q>0} W(k,q,q,k)v_5(k;t)v_5^*(q;t) \\
&+ 4Ui\sum_{q>0} W(q,k,k,q)v_5(q;t)v_5^*(k;t) \\
&+ 4Ui\sum_{q>0} W(k,\bar{k},q,\bar{q})v_6(\bar{k};t)v_6^*(q;t) \\
&- 4Ui\sum_{q>0} W(q,\bar{q},k,\bar{k})v_6(q;t)v_6^*(\bar{k};t), \qquad \text{(D6)}
\end{aligned}$$

$$\begin{aligned}
\dot{v}_3(k;t) &= -i\cos(k)\left(v_6(k;t) + v_6(\bar{k},t)\right) \\
&+ \gamma\sin(k)\left(v_5(k;t) - v_5(\bar{k},t)\right) - 2ihv_3(k;t) \\
&+ 4Ui\sum_{q>0} W(k,q,k,q)v_2(q;t)v_3(k;t) \\
&+ 4Ui\sum_{q>0} W(q,\bar{k},\bar{k},q)v_5(q;t)v_6(k;t) \\
&- 4Ui\sum_{q>0} W(\bar{k},q,\bar{k},q)v_2(q;t)v_3(\bar{k};t) \\
&+ 4Ui\sum_{q>0} W(q,k,k,q)v_5(q;t)v_6(\bar{k};t) \\
&- 4Ui\sum_{q>0} W(q,\bar{q},\bar{k},k)v_6(q;t)v_5(k;t) \\
&- 4Ui\sum_{q>0} W(q,\bar{q},k,\bar{k})v_6(q;t)v_5(\bar{k};t), \qquad \text{(D7)}
\end{aligned}$$

$$\begin{aligned}
\dot{v}_4(k;t) &= i\cos(k)\left(v_6(k;t) + v_6(\bar{k},t)\right) \\
&- \gamma\sin(k)\left(v_5(k;t) - v_5(\bar{k},t)\right) + 2ihv_4(k;t) \\
&- 4Ui\sum_{q>0} W(q,\bar{q},k,\bar{k})v_6(q;t)v_5^*(k;t) \\
&+ 4Ui\sum_{q>0} W(\bar{k},q,q,\bar{k})v_5^*(q;t)v_6(\bar{k};t) \\
&- 4Ui\sum_{q>0} W(\bar{k},q,\bar{k},q)v_1(q;t)v_4(\bar{k};t) \\
&+ 4Ui\sum_{q>0} W(k,q,k,q)v_1(q;t)v_4(k;t) \\
&- 4Ui\sum_{q>0} W(q,\bar{q},\bar{k},k)v_6(q;t)v_5^*(\bar{k};t) \\
&+ 4Ui\sum_{q>0} W(k,q,q,k)v_5^*(q;t)v_6(k;t), \qquad \text{(D8)}
\end{aligned}$$

$$\begin{aligned}
\dot{v}_5(k;t) &= i\cos(k)\left(v_2(k;t) - v_1(k;t)\right) \\
&+ \gamma\sin(k)\left(v_4^*(k;t) - v_3(k;t)\right) \\
&- 4Ui\sum_{q>0} W(q,k,q,k)v_1(q;t)v_5(k;t) \\
&+ 4Ui\sum_{q>0} W(k,q,k,q)v_2(q;t)v_5(k;t) \\
&+ 4Ui\sum_{q>0} W(q,k,k,q)v_1(k;t)v_5(q;t) \\
&- 4Ui\sum_{q>0} W(q,\bar{q},k,\bar{k})v_4^*(q;t)v_6(\bar{k};t) \\
&- 4Ui\sum_{q>0} W(\bar{k},k,q,\bar{q})v_3(q;t)v_6^*(k;t) \\
&- 4Ui\sum_{q>0} W(q,k,k,q)v_2(k;t)v_5(q;t), \qquad \text{(D9)}
\end{aligned}$$

$$\begin{aligned}
\dot{v}_6(k;t) &= i\cos(k)\left(v_4(k;t) - v_3(k;t)\right) \\
&- \gamma\sin(k)\left(v_1(k;t) + v_2(\bar{k};t) - 1\right) + 2ihv_6(k;t)) \\
&- 4Ui\sum_{q>0} W(q,\bar{q},k,\bar{k})v_6(q;t)v_1(k;t) \\
&+ 4Ui\sum_{q>0} W(k,q,k,q)v_2(q;t)v_6(k;t) \\
&+ 4Ui\sum_{q>0} W(\bar{k},q,\bar{k},q)v_1(q;t)v_6(k;t) \\
&- 4Ui\sum_{q>0} W(q,k,k,q)v_5(q;t)v_4(k;t) \\
&+ 4Ui\sum_{q>0} W(q,\bar{q},k,\bar{k})v_6(q;t)(1 - v_2(\bar{k};t)) \\
&+ 4Ui\sum_{q>0} W(\bar{k},q,q,\bar{k})v_5^*(q;t)v_3(k;t)\,. \qquad \text{(D10)}
\end{aligned}$$

[1] A. Polkovnikov, K. Sengupta, A. Silva, and M. Vengalattore, *Colloquium: Nonequilibrium dynamics of closed interacting quantum systems*, Rev. Mod. Phys. **83**, 863

(2011).
[2] C. Gogolin and J. Eisert, *Equilibration, thermalisation, and the emergence of statistical mechanics in closed quantum systems*, Rep. Prog. Phys. **79**, 056001 (2016).
[3] L. D'Alessio, Y. Kafri, A. Polkovnikov, and M. Rigol, *From Quantum Chaos and Eigenstate Thermalization to Statistical Mechanics and Thermodynamics*, arXiv:1509.06411 (2015).
[4] P. Calabrese and J. Cardy, *Quantum quenches in 1+1 dimensional conformal field theories*, J. Stat. Mech. (2016) 064003.
[5] J.-S. Caux, *The Quench Action*, J. Stat. Mech. (2016) 064006.
[6] M. A. Cazalilla and M.-C. Chung, *Quantum Quenches in the Luttinger model and its close relatives*, J. Stat. Mech. (2016) 064004.
[7] F. H. L. Essler and M. Fagotti, *Quench dynamics and relaxation in isolated integrable quantum spin chains*, J. Stat. Mech. (2016) 064002.
[8] A. De Luca and G. Mussardo, *Equilibration Properties of Classical Integrable Field Theories*, J. Stat. Mech. (2016) 0640011.
[9] D. Bernard and B. Doyon, *Conformal field theory out of equilibrium: a review*, J. Stat. Mech. (2016) 064005.
[10] R. Vasseur and J. E. Moore, *Nonequilibrium quantum dynamics and transport: from integrability to many-body localization*, J. Stat. Mech. (2016) 064010.
[11] T. Langen, T. Gasenzer, and J. Schmiedmayer, *Prethermalization and universal dynamics in near-integrable quantum systems*, J. Stat. Mech. (2016) 064009.
[12] L. Vidmar and M. Rigol, *Generalized Gibbs ensemble in integrable lattice models*, J. Stat. Mech. (2016) 064007.
[13] M. Rigol, *Fundamental Asymmetry in Quenches Between Integrable and Nonintegrable Systems*, Phys. Rev. Lett. **116**, 100601 (2016).
[14] J. M. Deutsch, *Quantum statistical mechanics in a closed system*, Phys. Rev. A **43**, 2046 (1991).
[15] M. Srednicki, *Chaos and quantum thermalization*, Phys. Rev. E **50**, 888 (1994).
[16] M. Rigol V. Dunjko, and M. Olshanii, *Thermalization and its mechanism for generic isolated quantum systems*, Nature **452**, 854 (2008).
[17] M. Rigol, *Breakdown of Thermalization in Finite One-Dimensional Systems*, Phys. Rev. Lett. **103**, 100403 (2009).
[18] M. Rigol and L. F. Santos, *Quantum chaos and thermalization in gapped systems*, Phys. Rev. A **82**, 011604(R) (2010).
[19] G. Biroli, C. Kollath, and A. M. Läuchli, *Effect of Rare Fluctuations on the Thermalization of Isolated Quantum Systems*, Phys. Rev. Lett. **105**, 250401 (2010).
[20] M. C. Bañuls, J. I. Cirac, and M. B. Hastings, *Strong and Weak Thermalization of Infinite Nonintegrable Quantum Systems*, Phys. Rev. Lett. **106**, 050405 (2011).
[21] M. Tavora and A. Mitra, *Quench dynamics of one-dimensional bosons in a commensurate periodic potential: A quantum kinetic equation approach*, Phys. Rev. B **88**, 115144 (2013).
[22] M. Rigol, *Quantum Quenches in the Thermodynamic Limit*, Phys. Rev. Lett. **112**, 170601 (2014).
[23] M. Rigol, V. Dunjko, V. Yurovsky, and M. Olshanii, *Relaxation in a Completely Integrable Many-Body Quantum System: An Ab Initio Study of the Dynamics of the Highly Excited States of 1D Lattice Hard-Core Bosons*, Phys. Rev. Lett. **98**, 050405 (2007).
[24] M. Rigol, A. Muramatsu, and M. Olshanii, *Hard-core bosons on optical superlattices: Dynamics and relaxation in the superfluid and insulating regimes* Phys. Rev. A **74**, 053616 (2006).
[25] M. A. Cazalilla, *Effect of Suddenly Turning on Interactions in the Luttinger Model*, Phys. Rev. Lett. **97**, 156403 (2006).
[26] P. Calabrese and J. Cardy, *Quantum quenches in extended systems*, J. Stat. Mech. (2007) P06008.
[27] M. Cramer, C. M. Dawson, J. Eisert, and T. J. Osborne, *Exact Relaxation in a Class of Nonequilibrium Quantum Lattice Systems*, Phys. Rev. Lett. **100**, 030602 (2008).
[28] T. Barthel and U. Schollwöck, *Dephasing and the Steady State in Quantum Many-Particle Systems*, Phys. Rev. Lett. **100**, 100601 (2008).
[29] D. Fioretto and G. Mussardo, *Quantum quenches in integrable field theories*, New J. Phys. **12**, 055015 (2010).
[30] B. Pozsgay, *Mean values of local operators in highly excited Bethe states*, J. Stat. Mech. (2011) P01011.
[31] P. Calabrese, F. H. L. Essler, and M. Fagotti, *Quantum Quench in the Transverse-Field Ising Chain*, Phys. Rev. Lett. **106**, 227203 (2011); *Quantum quenches in the transverse field Ising chain: II. Stationary state properties*, J. Stat. Mech. (2012) P07022.
[32] B. Dóra, Á. Bácsi, and G. Zaránd, *Generalized Gibbs ensemble and work statistics of a quenched Luttinger liquid*, Phys. Rev. B **86**, 161109(R) (2012).
[33] J.-S. Caux and R. M. Konik, *Constructing the Generalized Gibbs Ensemble after a Quantum Quench*, Phys. Rev. Lett. **109**, 175301 (2012).
[34] F. H. L. Essler, S. Evangelisti, and M. Fagotti, *Dynamical Correlations After a Quantum Quench*, Phys. Rev. Lett. **109**, 247206 (2012).
[35] M. Fagotti and F. H. L. Essler, *Reduced density matrix after a quantum quench*, Phys. Rev. B **87**, 245107 (2013).
[36] M. Collura, S. Sotiriadis, and P. Calabrese, *Equilibration of a Tonks-Girardeau Gas Following a Trap Release*, Phys. Rev. Lett. **110**, 245301 (2013); *Quench dynamics of a TonksGirardeau gas released from a harmonic trap*, J. Stat. Mech. (2013) P09025.
[37] J.-S. Caux and F. H. L. Essler, *Time Evolution of Local Observables After Quenching to an Integrable Model*, Phys. Rev. Lett. **110**, 257203 (2013).
[38] G. Mussardo, *Infinite-Time Average of Local Fields in an Integrable Quantum Field Theory After a Quantum Quench*, Phys. Rev. Lett. **111**, 100401 (2013).
[39] B. Pozsgay, *The generalized Gibbs ensemble for Heisenberg spin chains*, J. Stat. Mech. (2013) P07003.
[40] M. Kormos, A. Shashi, Y.-Z. Chou, J.-S. Caux and A. Imambekov, *Interaction quenches in the one-dimensional Bose gas*, Phys. Rev. B **88**, 205131 (2013).
[41] M. Fagotti and F. H. L. Essler, *Stationary behaviour of observables after a quantum quench in the spin-1/2 Heisenberg XXZ chain* J. Stat. Mech. (2013) P07012.
[42] L. Bucciantini, M. Kormos, and P. Calabrese, *Quantum quenches from excited states in the Ising chain*, J. Phys. A **47**, 175002 (2014).
[43] M. Fagotti, M. Collura, F. H. L. Essler, and P. Calabrese, *Relaxation after quantum quenches in the spin-1/2 Heisenberg XXZ chain*, Phys. Rev. B **89**, 125101 (2014).
[44] B. Wouters, J. De Nardis, M. Brockmann, D. Fioretto, M. Rigol, and J.-S. Caux, *Quenching the Anisotropic*

Heisenberg Chain: Exact Solution and Generalized Gibbs Ensemble Predictions, Phys. Rev. Lett. **113**, 117202 (2014).

[45] B. Pozsgay, M. Mestyán, M. A. Werner, M. Kormos, G. Zaránd, and G. Takács, *Correlations after Quantum Quenches in the XXZ Spin Chain: Failure of the Generalized Gibbs Ensemble*, Phys. Rev. Lett. **113**, 117203 (2014).

[46] M. Kormos, M. Collura, and P. Calabrese, *Analytic results for a quantum quench from free to hard-core one-dimensional bosons*, Phys. Rev. A **89**, 013609 (2014).

[47] J. De Nardis, B. Wouters, M. Brockmann, and J.-S. Caux, *Solution for an interaction quench in the Lieb-Liniger Bose gas*, Phys. Rev. A **89**, 033601 (2014).

[48] S. Sotiriadis and P. Calabrese, *Validity of the GGE for quantum quenches from interacting to noninteracting models*, J. Stat. Mech. (2014) P07024.

[49] G. Goldstein and N. Andrei, *Failure of the local generalized Gibbs ensemble for integrable models with bound states*, Phys. Rev. A **90**, 043625 (2014).

[50] M. Brockmann, B. Wouters, D. Fioretto, J. De. Nardis, R. Vlijm, and J.-S. Caux, *Quench action approach for releasing the Néel state into the spin-1/2 XXZ chain*, J. Stat. Mech. (2014) P12009.

[51] B. Pozsgay, *Quantum quenches and Generalized Gibbs Ensemble in a Bethe Ansatz solvable lattice model of interacting bosons*, J. Stat. Mech. (2014) P10045.

[52] M. Mestyán, B. Pozsgay, G. Takács, and M. A. Werner, *Quenching the XXZ spin chain: quench action approach versus generalized Gibbs ensemble*, J. Stat. Mech. (2015) P04001.

[53] F. H. L. Essler, G. Mussardo, and M. Panfil, *Generalized Gibbs ensembles for quantum field theories*, Phys. Rev. A **91**, 051602(R) (2015).

[54] E. Ilievski, J. De Nardis, B. Wouters, J.-S. Caux, F. H. L. Essler, and T. Prosen, *Complete Generalized Gibbs Ensembles in an Interacting Theory*, Phys. Rev. Lett. **115**, 157201 (2015).

[55] S. Sotiriadis, *Memory-preserving equilibration after a quantum quench in a 1d critical model*, arXiv:1507.07915 (2015).

[56] E. Ilievski, E. Quinn, J. De Nardis, and M. Brockmann, *String-charge duality in integrable lattice models*, J. Stat. Mech. (2016) 063101.

[57] L. Piroli, P. Calabrese, and F. H. L. Essler, *Multiparticle Bound-State Formation following a Quantum Quench to the One-Dimensional Bose Gas with Attractive Interactions*, Phys. Rev. Lett. **116**, 070408 (2016); *Quantum quenches to the attractive one-dimensional Bose gas: exact results*, arXiv:1604.08141 (2016).

[58] B. Bertini, L. Piroli, and P. Calabrese, *Quantum quenches in the sinh-Gordon model: steady state and one-point correlation functions*, J. Stat. Mech. (2016) 063102.

[59] L. Piroli, E. Vernier, P. Calabrese, *Exact steady states for quantum quenches in integrable Heisenberg spin chains*, arXiv:1606.00383 (2016).

[60] A. Bastianello, S. Sotiriadis, *Quasi locality of the GGE in interacting-to-free quenches in relativistic field theories*, arXiv:1608.00924 (2016).

[61] V. I. Arnold, *Mathematical Methods of Classical Mechanics*, Springer, New York, 1989.

[62] M. Moeckel and S. Kehrein, *Interaction Quench in the Hubbard Model*, Phys. Rev. Lett. **100**, 175702 (2008); *Real-time evolution for weak interaction quenches in quantum systems*, Ann. Phys. **324**, 2146 (2009).

[63] A. Rosch, D. Rasch, B. Binz, and M. Vojta, *Metastable Superfluidity of Repulsive Fermionic Atoms in Optical Lattices*, Phys. Rev. Lett. **101**, 265301 (2008).

[64] M. Kollar, F. A. Wolf, and M. Eckstein, *Generalized Gibbs ensemble prediction of prethermalization plateaus and their relation to nonthermal steady states in integrable systems*, Phys. Rev. B **84**, 054304 (2011).

[65] M. van den Worm, B. C. Sawyer, J. J. Bollinger, and M. Kastner, *Relaxation timescales and decay of correlations in a long-range interacting quantum simulator*, New J. Phys. **15**, 083007 (2013).

[66] M. Marcuzzi, J. Marino, A. Gambassi, and A. Silva, *Prethermalization in a Nonintegrable Quantum Spin Chain after a Quench*, Phys. Rev. Lett. **111**, 197203 (2013).

[67] F. H. L. Essler, S. Kehrein, S. R. Manmana, and N. J. Robinson, *Quench dynamics in a model with tuneable integrability breaking*, Phys. Rev. B **89**, 165104 (2014).

[68] N. Nessi, A. Iucci and M. A. Cazalilla, *Quantum Quench and Prethermalization Dynamics in a Two-Dimensional Fermi Gas with Long-Range Interactions*, Phys. Rev. Lett. **113**, 210402 (2014).

[69] M. Fagotti, *On conservation laws, relaxation and pre-relaxation after a quantum quench*, J. Stat. Mech. (2014) P03016.

[70] G. P. Brandino, J.-S. Caux, and R. M. Konik, *Glimmers of a Quantum KAM Theorem: Insights from Quantum Quenches in One-Dimensional Bose Gases*, Phys. Rev. X **5**, 041043 (2015).

[71] B. Bertini and M. Fagotti, *Pre-relaxation in weakly interacting models*, J. Stat. Mech. (2015) P07012.

[72] A. Chiocchetta, M. Tavora, A. Gambassi, and A. Mitra, *Short-time universal scaling in an isolated quantum system after a quench*, Phys. Rev. B **91**, 220302(R) (2015); Phys. Rev. **B** 92, 219901(E) (2015).

[73] M. Babadi, E. Demler, and M. Knap, *Far-from-Equilibrium Field Theory of Many-Body Quantum Spin Systems: Prethermalization and Relaxation of Spin Spiral States in Three Dimensions*, Phys. Rev. X **5**, 041005 (2015).

[74] P. Smacchia, M. Knap, E. Demler, and A. Silva, *Exploring dynamical phase transitions and prethermalization with quantum noise of excitations*, Phys. Rev. B **91**, 205136 (2015).

[75] B. Bertini, F. H. L. Essler, S. Groha, and N. J. Robinson, *Prethermalization and Thermalization in Models with Weak Integrability Breaking*, Phys. Rev. Lett. **115**, 180601 (2015).

[76] M. Fagotti and M. Collura, *Universal prethermalization dynamics of entanglement entropies after a global quench*, arXiv:1507.02678 (2015).

[77] G. Menegoz and A. Silva, *Prethermalization of weakly interacting bosons after a sudden interaction quench*, J. Stat. Mech. (2015) P05035.

[78] E. Kaminishi, T. Mori, T. Ikeda, N. Tatsuhiko, and M. Ueda, *Entanglement pre-thermalization in a one-dimensional Bose gas*, Nat. Phys. **11**, 1050 (2015).

[79] G. Delfino, *Quantum quenches with integrable pre-quench dynamics*, J. Phys. A **47** (2014) 402001.

[80] T. Kitagawa, A. Imambekov, J. Schmiedmayer, and E. Demler, *The dynamics and prethermalization of one-dimensional quantum systems probed through the full dis-*

tributions of quantum noise, New J. Phys. **13**, 073018 (2011).

[81] M. Gring, M. Kuhnert, T. Langen, T. Kitagawa, B. Rauer, M. Schreitl, I. Mazets, D. Adu Smith, E. Demler, and J. Schmiedmayer, *Relaxation and Prethermalization in an Isolated Quantum System*, Science **337**, 1318 (2012).

[82] D. Adu Smith, M. Gring, T. Langen, M. Kuhnert, B. Rauer, R. Geiger, T. Kitagawa, I. Mazets, E. Demler, and J. Schmiedmayer, *Prethermalization revealed by the relaxation dynamics of full distribution functions*, New J. Phys. **15** 075011 (2013).

[83] T. Langen, M. Gring, M. Kuhnert, B. Rauer, R. Geiger, D. A. Smith, I. E. Mazets, and J. Schmiedmayer, *Prethermalization in one-dimensional Bose gases: Description by a stochastic Ornstein-Uhlenbeck process*, Eur. Phys. J. Special Topics **217**, 43 (2013).

[84] U. Schollwöck, *The density-matrix renormalization group*, Rev. Mod. Phys. **77**, 259 (2005).

[85] M. Stark and M. Kollar, *Kinetic description of thermalization dynamics in weakly interacting quantum systems*, arXiv:1308.1610 (2013).

[86] R. Orbach, *Linear Antiferromagnetic Chain with Anisotropic Coupling*, Phys. Rev. **112**, 309 (1958).

[87] F. H. L. Essler and R. M. Konik in *From Fields to Strings: Circumnavigating Theoretical Physics*, edited by M. Shifman, A. Vainshtein, and J. Wheater (World Scientific, Singapore, 2005); *Applications of Massive Integrable Quantum Field Theories to Problems in Condensed Matter Physics*, arXiv:0412421 (2004).

[88] N. Nessi and A. Iucci, *Glass-like Behavior in a System of One Dimensional Fermions after a Quantum Quench*, arXiv:1503.02507 (2015).

[89] A. Iucci and N. Nessi, *Equations of Motion for the Out-of-Equilibrium Dynamics of Isolated Quantum Systems from the Projection Operator Technique*, J. Phys.: Conf. Ser. **568**, 012013 (2014).

[90] L. Erdős, M. Salmhofer, and H.-T. Yau, *On the Quantum Boltzmann Equation*, J. Stat. Phys. **116**, 367 (2004).

[91] M. Bonitz, *Quantum Kinetic Theory* (Teubner, Stuttgart, 1998).

[92] L. P. Kadanoff and G. A. Baym, *Quantum statistical mechanics* (Benjamin, New York, 1962).

[93] S. Hermanns, K. Balzer, and M. Bonitz, *Few-particle quantum dynamicscomparing nonequilibrium Green functions with the generalized KadanoffBaym ansatz to density operator theory*, J. Phys.: Conf. Ser. **427** 012008 (2013).

[94] J. Lukkarinen and H. Spohn, *Not to Normal Order–Notes on the Kinetic Limit for Weakly Interacting Quantum Fluids*, J. Stat. Phys. **134**, 1133 (2009).

[95] W. H. Press, S. A. Teukolsky, W. T. Vetterling, B. P. Flannery, *Numerical Recipes: The Art of Scientific Computing*, Third Edition, Cambridge University Press, Cambridge, 2007.

[96] J. Lux, J. Müller, A. Mitra, A. Rosch, *Hydrodynamic long-time tails after a quantum quench*, Phys. Rev. A **89**, 053608 (2014).

[97] H. Kim, M. C. Banuls, J. I. Cirac, M. B. Hastings, and D. A. Huse, *Slowest local operators in quantum spin chains*, Phys. Rev. E **92** 012128 (2015).

[98] F. Wegner, *Flow-equations for Hamiltonians*, Ann. Physik **506**, 77 (1994).

[99] C. Knetter and G. S. Uhrig, *Perturbation theory by flow equations: dimerized and frustrated S = 1/2 chain*, Eur. Phys. J. B **13**, 2 (2000); C. P. Heidbrink and G. S. Uhrig, *Renormalization by continuous unitary transformations: one-dimensional spinless fermions*, Eur. Phys. J. B **30**, 4 (2002).

[100] S. Kehrein, *The flow-equation approach to many-particle systems* (Springer, Berlin, 2007).

[101] M. L. R. Fürst, C. B. Mendl, and H. Spohn, *Matrix-valued Boltzmann equation for the nonintegrable Hubbard chain*, Phys. Rev. E **88**, 012108 (2013).

[102] F. R. A. Biebl and S. Kehrein, *Thermalization rates in the one dimensional Hubbard model with next-to-nearest neighbor hopping*, arXiv:1607.07115 (2016).

[103] M. Rigol and M. Fitzpatrick, *Initial-state dependence of the quench dynamics in integrable quantum systems*, Phys. Rev. A **84**, 033640 (2011).

[104] K. He and M. Rigol, *Initial-state dependence of the quench dynamics in integrable quantum systems. II. Thermal states*, Phys. Rev. A **85**, 063609 (2012).

[105] K. He and M. Rigol, *Initial-state dependence of the quench dynamics in integrable quantum systems. III. Chaotic states*, Phys. Rev. A **87**, 043615 (2013).

[106] E. J. Torres-Herrera and L. F. Santos, *Effects of the interplay between initial state and Hamiltonian on the thermalization of isolated quantum many-body systems*, Phys. Rev. E **88**, 042121 (2013).

[107] We do not plot $\tau^{-1}(L/2, L/2+1)$ because large oscillations and slow decay cause very large errors in the fit.

[108] P. Calabrese and J. Cardy, *Evolution of entanglement entropy in one-dimensional systems*, J. Stat. Mech. (2005) P04010.

[109] G. De Chiara, S. Montangero, P. Calabrese, and R. Fazio, *Entanglement entropy dynamics of Heisenberg chains*, J. Stat. Mech. (2006) P03001.

[110] A. Läuchli and C. Kollath, *Spreading of correlations and entanglement after a quench in the one-dimensional Bose–Hubbard model*, J. Stat. Mech. (2008) P05018.

[111] M. Fagotti and P. Calabrese, *Evolution of entanglement entropy following a quantum quench: Analytic results for the XY chain in a transverse magnetic field*, Phys. Rev. A **78**, 010306(R) (2008).

[112] S. R. Manmana, S. Wessel, R. M. Noack, and A. Muramatsu, *Time evolution of correlations in strongly interacting fermions after a quantum quench*, Phys. Rev. B **79**, 155104 (2009).

[113] M. Cheneau, P. Barmettler, D. Poletti, M. Endres, P. Schauss, T. Fukuhara, C. Gross, I. Bloch, C. Kollath, and S. Kuhr, *Light-cone-like spreading of correlations in a quantum many-body system*, Nature **481**, 484 (2012).

[114] T. Langen, R. Geiger, M. Kuhnert, B. Rauer, and J. Schmiedmayer, *Local emergence of thermal correlations in an isolated quantum many-body system*, Nature Phys. **9**, 640 (2013).

[115] L. Bonnes, F. H. L. Essler and A. Läuchli, *"Light-Cone" Dynamics After Quantum Quenches in Spin Chains*, Phys. Rev. Lett. **113**, 187203 (2014).

[116] K. V. Krutitsky, P. Navez, F. Queisser, and R. Schützhold, *Propagation of quantum correlations after a quench in the Mott-insulator regime of the Bose-Hubbard model*, EPJ Quantum Technol. **1**, 1 (2014).

[117] M. Fagotti, *Control of global properties in a closed many-body quantum system by means of a local switch*, arXiv:1508.04401 (2015).

[118] B. Bertini and M. Fagotti, *Determination of the nonequilibrium steady state emerging from a defect*, Phys.

Rev. Lett. 117, 130402 (2016).

[119] O. A. Castro-Alvaredo, B. Doyon, and T. Yoshimura, *Emergent hydrodynamics in integrable quantum systems out of equilibrium*, arXiv:1605.07331 (2016).

[120] B. Bertini, M. Collura, J. De Nardis, and M. Fagotti, *Transport in out-of-equilibrium XXZ chains: exact profiles of charges and currents*, Phys. Rev. Lett. **117**, 207201 (2016).

[121] M. Ganahl, E. Rabel, F.H.L. Essler and H.-G. Evertz, *Observation of Complex Bound States in the Spin-1/2 Heisenberg XXZ Chain Using Local Quantum Quenches*, Phys. Rev. Lett. **108**, 077206 (2012).

[122] J. Cardy, *Quantum quenches to a critical point in one dimension: some further results*, J. Stat. Mech. (2016) 023103.

[123] M. Kormos, M. Collura, G. Takács, and P. Calabrese, *Real time confinement following a quantum quench to a non-integrable model*, arXiv:1604.03571 (2016).

[124] M. Abramowitz, I. A. Stegun, *Handbook of Mathematical Functions: with formulas, graphs, and mathematical tables*, Vol. 55. Courier Corporation, 1964.

[125] V. Hunyadi, Z. Rácz, and L. Sasvári, *Dynamic scaling of fronts in the quantum XX chain*, Phys. Rev. E **69**, 066103 (2004).

[126] V. Eisler and Z. Rácz, *Full Counting Statistics in a Propagating Quantum Front and Random Matrix Spectra*, Phys. Rev. Lett. **110**, 060602 (2013).

[127] J. Viti, J.-M. Stéphan, J. Dubail, M. Haque, *Inhomogeneous quenches in a fermionic chain: exact results*, arXiv:1507.08132 (2015).

[128] D. Bernard and B. Doyon, *A hydrodynamic approach to non-equilibrium conformal field theories*, J. Stat. Mech. (2016) 033104.

[129] M. L. R. Fürst, C. B. Mendl, and H. Spohn, *Matrix-valued Boltzmann equation for the Hubbard chain*, Phys. Rev. E **86**, 031122 (2012).

[130] T. M. Wright, M. Rigol, M. J. Davis, and K. V. Kheruntsyan, *Nonequilibrium Dynamics of One-Dimensional Hard-Core Anyons Following a Quench: Complete Relaxation of One-Body Observables*, Phys. Rev. Lett. **113**, 050601 (2014).

[131] C. K. Majumdar and D. K. Ghosh, *On Next-Nearest-Neighbor Interaction in Linear Chain. I*, J. Math. Phys. **10**, 1388 (1969).

[132] B. M. McCoy and T. T. Wu, *Two-dimensional Ising field theory in a magnetic field: Breakup of the cut in the two-point function*, Phys. Rev. D **18**, 1259 (1978).

[133] T. Rakovszky, M. Mestyán, M. Collura, M. Kormos, and G. Takács, *Hamiltonian truncation approach to quenches in the Ising field theory*, arXiv:1607.01068 (2016).